1-1-2013

The Effects of Mean Sea Level and Tidal Amplitude On Ground Water Discharge and Pore-Water Salinity Distribution Along A Forest/Marsh Boundary, North Inlet, SC

John Bradley Peurifoy
University of South Carolina - Columbia

THE EFFECTS OF MEAN SEA LEVEL AND TIDAL AMPLITUDE ON GROUND WATER DISCHARGE AND PORE-WATER SALINITY DISTRIBUTION ALONG A FOREST/MARSH BOUNDARY, NORTH INLET, SC

by

John B. Peurifoy

Bachelor of Science
University of South Carolina, 2007

Submitted in Partial Fulfillment of the Requirements

For the Degree of Master of Science in

Geological Sciences

College of Arts and Sciences

University of South Carolina

2013

Accepted by:

Alicia M. Wilson, Director of Thesis

Scott M. White, Reader

James Morris, Reader

Lacy Ford, Vice Provost and Dean of Graduate Studies

DEDICATION

This thesis and graduate degree are dedicated to my daughter Madelyn Grae Peurifoy and my grandmother, the late Frances Peurifoy.

ACKNOWLEDGEMENTS

I would like to sincerely thank Alicia Wilson for allowing me to complete my Master's degree under her guidance. Thank you for being patient with me throughout this process and for imparting your knowledge of groundwater processes and numerical modeling to me. You have been and will continue to be an exceptional teacher, advisor and friend. Many thanks are also due to my lab mates Andrea Hughes and Tyler Evans. Both of you have provided me with valuable insights into my research and countless hours of enjoyable conversation. It has been a pleasure getting to know you both, and I wish you all the best in your future endeavors.

ABSTRACT

Advective groundwater flow in salt marshes is an important mechanism through which nutrients are exported to adjacent coastal waters. Groundwater flow also influences the distribution of pore-water salinity in the subsurface marsh, which affects botanical zonation, nutrient transport, and primary productivity. Recent idealized marsh island simulations have suggested that increases in tidal amplitude result in increased groundwater discharge, and that the elevation of MWL relative to the marsh platform is inversely related to groundwater discharge. These simulations were only representative of marsh islands (as opposed to forest-marsh boundaries) and considered simple, idealized tides only. The results were not confirmed in a real field setting. This study utilized tidal records and hydraulic head records to calculate and compare groundwater discharge along two marsh environments: 1) a fringing marsh boundary that was influenced by a large freshwater lens and 2) a marsh island with a much smaller freshwater lens. Electrical resistivity surveys were conducted to image seasonal pore-water salinity distribution. The discharge trends were then correlated to trends in MWL and subsurface salinity. Our results indicated that discharge from the marsh to Crabhaul Creek was dependent on the position of MWL. Observations showed increases in groundwater discharge during periods of low MWL and decreases during periods of high MWL. In the

high marsh root zone, the occurrence and magnitude of discharge or recharge depended on precipitation, tidal amplitude and MWL. The electrical resistivity surveys depicted two distinct salinity zones, neither of which displayed any correlation to MWL or tidal amplitude. The first was a shallow tidally-influenced zone containing saline to brackish pore-water, and the second was a deeper freshwater flow zone. These results demonstrated the importance of MWL and tidal amplitude on discharge and hence nutrient export from salt marshes. It can be inferred that long-term sea level rise (at a rate that exceeds sediment accretion) will significantly decrease nutrient export from salt marshes.

TABLE OF CONTENTS

LIST OF TABLES

LIST OF FIGURES

LIST OF ABBREVIATIONS

AGI ..... Advanced Geosciences Incorporated

bgs ..... Below Ground Surface

ET ..... Evapotranspiration

IP ..... Induced Polarization

LTER ..... Long-Term Ecological Research

MWL ..... Mean Water Level

NERR ..... National Estuarine Research Reserve

NOAA ..... National Oceanic and Atmospheric Administration

NSF ..... National Science Foundation

ppt ..... Parts per Thousand

CHAPTER 1
INTRODUCTION

Forest-marsh boundaries are transitional environments between forested uplands and low-lying salt marshes that are typically located within the intertidal zone. Salt marshes in forest-marsh boundaries have the potential to regulate groundwater flow and nutrient fluxes between the terrestrial and marine systems. In coastal settings, maximum groundwater discharge occurs in intertidal and near-shore subtidal zones (Reilly and Goodman, 1985). Groundwater that is discharged from salt marshes is highly enriched with dissolved carbon, nutrients, metals, and radio-nuclides (Nixon, 1980). The nutrient-rich groundwater discharged by salt marshes can impact the fertility of adjacent coastal waters (Wilson and Morris, 2012), drive primary productivity (Morris, 1995) and can potentially cause phytoplankton blooms (Kelly and Moran, 2002).

The distribution of salinity in sediment pore-water is also an important factor in nutrient export and ecology. Subsurface salinity governs the ability of groundwater to transport nutrients. Nutrients tend to sorb to sediments if the salinity of the pore-water is less than 10 parts per thousand (ppt). Pore-water salinity also influences primary productivity (Morris, 1995) and has been determined to be influential in the botanical zonation of plant species that reside in salt marsh ecosystems (Thibodeau et al. 1997). Groundwater flow is the primary mechanism through which salts and nutrients are transported through the subsurface marsh (Krest et al, 2000).

Several processes govern advective groundwater flow in coastal salt marshes. These processes include evapotranspiration (ET), precipitation, input of groundwater from neighboring uplands, and variations in mean water level (MWL) and tidal amplitude (Wilson and Morris, 2012). There has been a recent interest in determining the rates at which groundwater discharges from subsurface marshes and which of the aforementioned processes are most influential in controlling the magnitude of that discharge.

Several studies have attempted to quantify discharge rates from salt marshes. Radium-isotope tracer (De Meneses, 1990; Krest et al. 2000), seepage meter (Whiting and Childers, 1989) and salt and water balance studies (Morris, 1995) have been used to determine the groundwater discharge rates for several coastal settings. These discharge values are variable and range from 0.15-15 L $m^{-2}d^{-1}$ (De Meneses, 1990) in the Pettaquamscutt River estuary to 7.8-40 L $m^{-2}d^{-1}$ in the North Inlet estuary (Whiting and Childers, 1989; Morris, 1995; Krest et al. 2000; and Wilson and Gardner, 2006).

Other studies have observed and attempted to explain variations in discharge on tidal, seasonal, and inter-annual scales (Tobias et al. 2001; Kelly and Moran, 2002; and Wilson and Morris, 2012). Tobias et al. (2001) and Kelly and Moran (2002) observed discharge rates over the course of one year for the Pettaquamscutt estuary and a fringing marsh located in southeastern Virginia, respectively. These studies showed that groundwater discharge in coastal areas is seasonally and inter-annually variable and concluded that variability was most likely related to variations in precipitation and ET. The observed precipitation and ET records did not wholly support this interpretation (Kelly and Moran, 2002). Furthermore, recent numerical simulations of idealized salt marsh islands have suggested that groundwater discharge is a function of the position of

MWL relative to the marsh surface and the amplitude of tidal cycles, with periods of high MWL decreasing discharge and larger tidal amplitudes generating more discharge (Wilson and Morris, 2012). These models were representative of marsh islands rather than forest-marsh boundaries where groundwater flow is thought to be influenced by large inputs of fresh terrestrial groundwater from the upland. Variations in discharge can lead to pulses of nutrient-rich groundwater being introduced into adjacent coastal waters and could be responsible for the occasional flushing of salts and nutrients from marsh sediments (Tobias et al. 2001). As of yet, no single process or combination of processes has been definitively identified as a control on these variations in groundwater discharge.

Seasonal salinity variations in salt marsh sediments have also been identified North Inlet, SC and have been attributed to precipitation, ET, infiltration of seawater during periods of inundation, and drainage (Morris, 1995). Carter et al. (2007) used electrical resistivity surveys to image the upper four meters of the subsurface marsh. The surveys revealed a fresh water plume at a depth of one to three meters below the marsh surface. The lateral extent of this plume migrated throughout the year. Carter et al. (2007) were unable to temporally correlate precipitation and ET data to changes in pore-water salinity. Similar variations in pore-water salinity were observed during a salinity sampling study conducted in a high marsh at North Inlet by Morris (1995). This study collected pore-water salinity samples from the shallow (one to 19 centimeters) subsurface marsh and produced monthly averages for a period ranging from 1987 to 1992. Significant inter-annual variability in pore-water salinity was observed and ranged from 23 to 43 parts per thousand (ppt). Morris (1995) proposed that salinity variations were driven primarily by infiltration, ET, and drainage. It was noted that the position of MWL

could impact the salinity values, and stated that future increases in MWL had the potential to greatly affect pore-water salinity (Morris, 1995).

The purpose of this study is to identify controls on groundwater discharge and subsurface salinity patterns across a forest/marsh boundary in North Inlet. We also aim to compare the magnitude of groundwater discharge in a forest/marsh system with those in a marsh island system. We hypothesize that groundwater discharge rates are directly related to the position of MWL and tidal amplitude and that groundwater discharge is the primary control on the distribution of salinity in the subsurface marsh. We further hypothesize that the groundwater discharge magnitudes associated with the forest/marsh environment are much greater than those associated with the marsh island environment. Monthly average discharge is calculated between four marsh locations and Crabhaul Creek using hydraulic head data from 1994 to 1995. Comparisons are made between average monthly discharge and the position of MWL, tidal amplitude, and precipitation. The calculated groundwater discharge values are compared with one another based on their location relative to Crabhaul Creek and the marsh system with which they were associated. Electrical resistivity surveys are also completed to image salinity distributions in the subsurface on June 30, 2012, August 1, 2012, January 11, 2012, and May 22, 2013. The electrical resistivity surveys are also compared to the position of MWL and precipitation.

CHAPTER 2
SITE LOCATION

The study site is located within the North Inlet Basin (Figure 2.1), which is approximately 11 miles east of Georgetown, SC. The North Inlet Basin is designated as a National Oceanic and Atmospheric Association (NOAA) National Estuarine Research Reserve (NERR) site and was also designated as a National Science Foundation (NSF) Long-Term Ecological Research (LTER) site from 1981 to 1993. As a result of these designations, long term tidal, meteorological, and hydrogeological data has been recorded for the site.

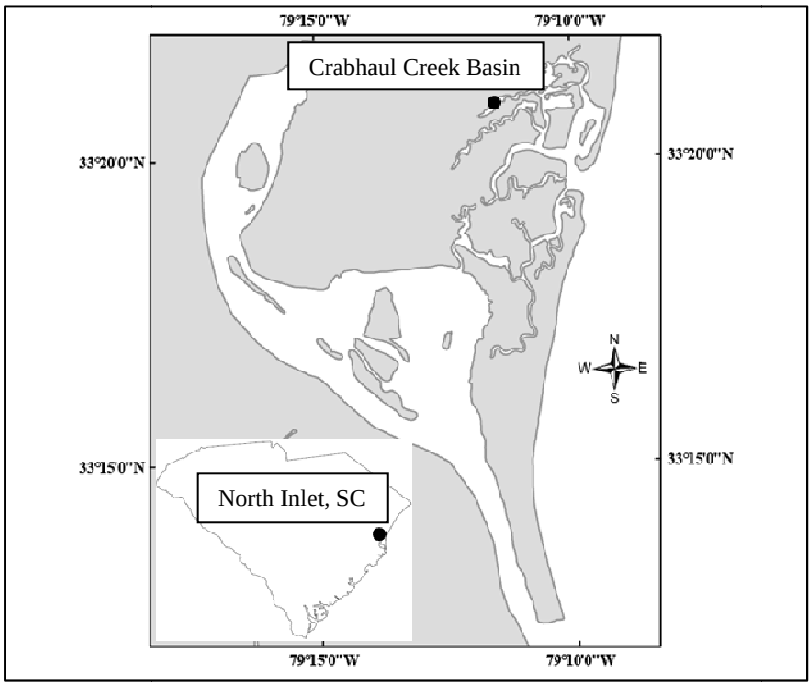

Figure 2.1 Geographic locations of North Inlet, SC and the Crabhaul Creek Basin.

The North Inlet Basin is a tidally-influenced, lagoonal estuary that is bordered to the south by Winyah Bay, to the east by the Atlantic Ocean, and to the north and west by low-lying forested uplands. The 32 km^2 basin experiences a semi-diurnal tide that has a period of 12.24 hours and a mean range of 1.5 meters (Gardner and Porter, 2001). The basin is hydraulically connected to the Atlantic Ocean through North Inlet and to a 75 km^2 terrestrial watershed across a 10 km forest-marsh boundary.

Our study focused on Transect D of Keenan (1994) and Thibodeau (1997), which is positioned along the forest-marsh boundary in the Crabhaul Creek Basin in the northwestern portion of the North Inlet Basin. The transect trends northwest to southeast across relict swale and is positioned orthogonal to the forest-marsh boundary and to Crabhaul Creek. Elevation along the transect ranges from 1.75 meters above MWL in the forested upland to -0.15 meters below MWL in the center of Crabhaul Creek. The transect extends 263 meters and contains a total of 29 groundwater monitoring well nests. Each nest contains three to five monitoring wells that range in depth from 0.6 to 4.88 meters below ground surface (bgs). The well nests are labeled alphanumerically based on their distance from the northwestern terminus of the transect.

The stratigraphy along Transect D (Figure 2.2) was logged during the installation of the monitoring wells by Keenan (1994) and Thibodeau (1997). A basal clay layer exists at a depth of three meters bgs in the upland and shallows to approximately 2.5 meters bgs near Crabhaul Creek. The basal clay unit shown in Figure 2.2 has been extrapolated based on stratigraphic data obtained with vibracores. The northwestern extent of the clay unit is a projection based on the available data. Fine to medium Pleistocene beach sands overlie the clay unit, which in turn is overlain by approximately

50 centimeters of marsh mud in the low- to high-marsh (Thibodeau, 1997). The sand unit, which is vertically bound by low permeability marsh mud and clay, forms a confined aquifer. Crabhaul Creek has incised a channel through the marsh mud and into the sands, which has created a conduit for fluid exchange between the confined aquifer of the marsh and the waters of the estuary.

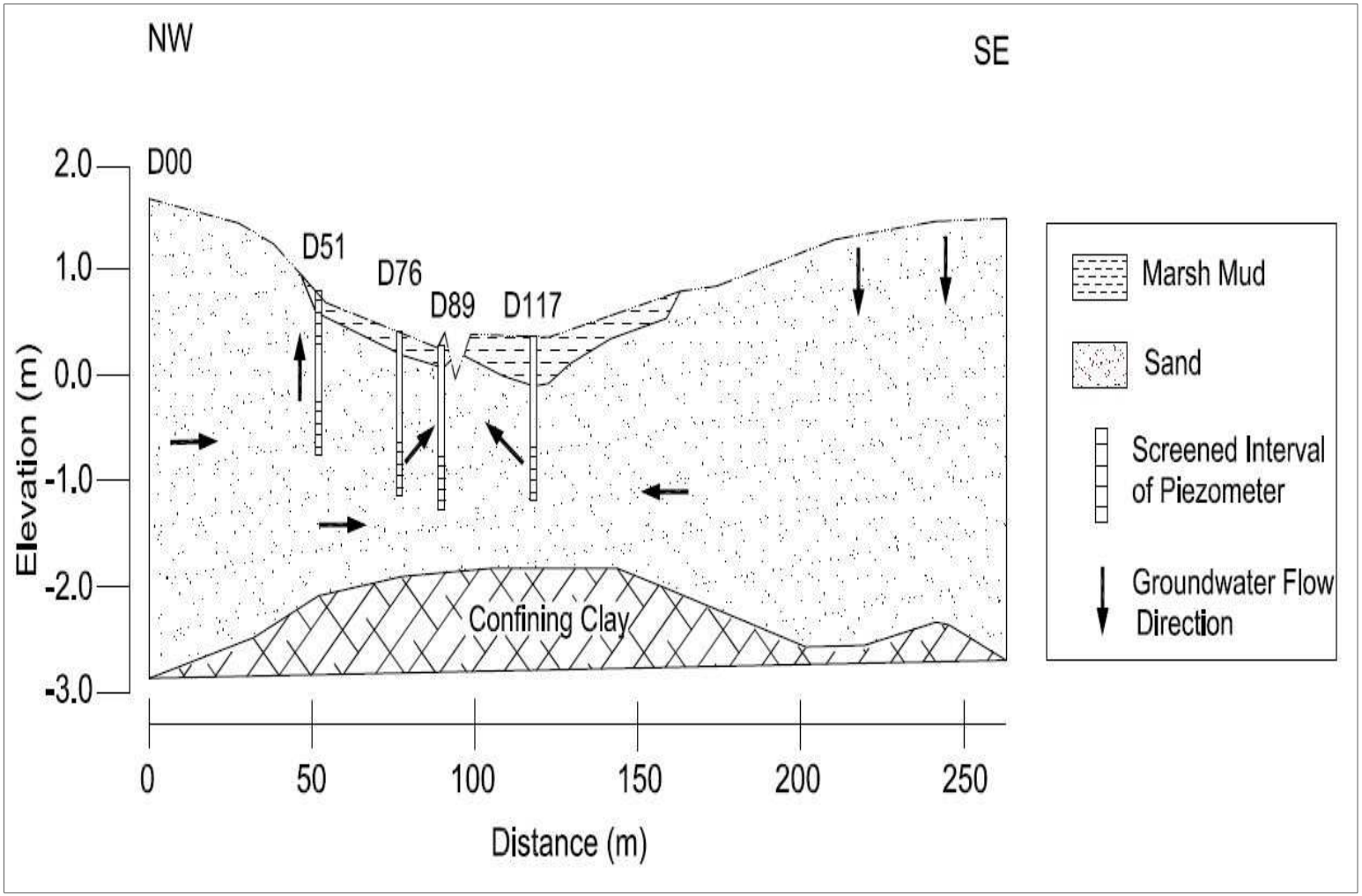

Figure 2.2 Cross-section of Transect D showing well nest location, geology, and groundwater flow direction.

CHAPTER 3
METHODOLOGY

3.1 Volumetric Flux, Net Flux, and Recharge

Darcy's Law can be written

$$Q = -KA\left(\frac{dh}{dx}\right) \qquad \text{(eq. 1)}$$

where Q is the volumetric flux (m^3d^{-1}), -K is the hydraulic conductivity (md^{-1}), A is the cross-sectional area through which flow occurs (m^2), *dh* is the difference between the total hydraulic head between two points of interest (m), and *dx* is the lateral distance between those two points (m). The values used in the calculations are provided in Table 3.1. We used eq. 1 to calculate volumetric flux using data from monitoring wells D76, D89, and D117 and Crabhaul Creek. We also used the equation to calculate the volumetric flux between two monitoring wells located at D51 that are screened at 0.6 and 3.6 meters bgs. These monitoring wells were chosen for the study because of the availability of historical data for the wells and their topographic location in the marsh (i.e. high, mid, and low-lying marsh). Semi-continuous, historical hydraulic head data is available for monitoring wells D51, D76, D89, and D117 from March 1, 1994 to May 1, 1996 (Thibodeau, 1997). The periods of record are not the same for each monitoring well, as indicated in Table 3.1. Verified historical tidal data from the Charleston, SC (station # 8665530) harbor has been obtained from the NOAA website at http://tidesandcurrents.noaa.gov for 1994 to 1996.

In the mid and low-marsh, experimentally determined hydraulic conductivity values are available for the sediments of the confined aquifer that immediately surround the screened intervals of D76, D89, and D117 (Thibodeau, 1997). The screened intervals of these wells are all located within the same confined aquifer, so we calculated the geometric mean of each of the experimental values to obtain one comprehensive value (5.08 md^{-1}) representative of the aquifer. In the high marsh, experimentally determined hydraulic conductivities are also available for the two screened intervals at D51 (Thibodeau, 1997). The geometric mean of these two values was also calculated to obtain one representative hydraulic conductivity value (1.96 md^{-1}). Using the aforementioned data and equation 1, volumetric fluxes are calculated between the two screened intervals of D51 and between D76, D89, and D117 and Crabhaul Creek.

Table 3.1 Volumetric flux calculation parameters

Well	K (m/d)	A (m^2)	dx (m)
D51	1.96	1	3
D76	5.08	0.31	18
D89	5.08	0.31	5
D117	5.08	0.29	23

On average, the volumetric flux values that we calculate for the mid-marsh at D76 are expected to be much lower than those that we calculate for the low-lying marsh at D89. This is a result of the propagation of tidal energy through the confined aquifer. Carr and van der Kamp (1969) showed that energy from fluctuating tides will propagate through confined aquifers that are in connection with tidally-influenced coastal waters. At

periods of high tide, the hydraulic head immediately adjacent to the creek bank is higher and is gradually damped with distance. The opposite is seen at periods of low tide. Hydraulic head is lower next to the creek bank and gradually rises to a higher hydraulic head as you approach the inland. This has impacted our discharge calculations by producing a greater range of values with larger magnitudes at the creek bank when compared with the mid-marsh. Thus, the fluxes reported for D76 and D117 do not represent discharge from the creek bank. They were chosen because, at comparable distances from the creek and with similar stratigraphy and permeability, they allowed us to compare fluxes on opposite sides of the creek.

Table 3.2 Hydraulic head data record for wells located along Transect D

Well ID	Period of Record
D51	March 1994 to February 1995
D76	March 1994 to November 1994
D89	March 1994 to April 1995
D117	June 1995 to January 1996

The net flux, total relative discharge and recharge are calculated between D89 and the center of Crabhaul Creek. In equation 1, K and *dx* are constant. A is also constant since the cross-sectional area that groundwater is being discharged from remains fully saturated even during periods of low tide. After assigning these constants, Q is proportional to *dh*. Thus, the sum of *dh* over tidal cycles yields relative flux per tidal cycle. A positive value denotes discharging groundwater and a negative value denotes recharging groundwater. The total discharge is calculated by summing the positive relative discharge values over a 12 hour tidal cycle. The net flux is the sum of both the

positive and negative discharge values. Recharge is the difference between total discharge and the net flux. Total discharge and net flux are calculated for each tidal cycle and then binned by month. We further bin the data according to the tidal amplitude.

3.2 Electrical Resistivity

Electrical resistivity surveys were completed along the northwestern portion of Transect D on June 30, 2012, August 1, 2012, January 11, 2013, and May 22, 2013. The survey lines begin at the northwestern end of Transect D at D00 and extend laterally to D117. The surveys were collected using an Advanced Geosciences, Inc. (AGI) Super Sting earth resistivity and induced polarization (IP) instrument. The electrodes were arranged in a 27 by four meter spread. The "roll along" method was employed during the surveys. The "roll along" method merges data from multiple surveys that are completed along the same line. At the beginning of each new survey, the initial electrode is moved progressively farther down the survey line allowing data points to overlap and data gaps to be filled. This is used when the lateral distance of interest is too large to be characterized by just one survey.

Electrical resistivity surveys provide a cross-section of the resistivity of the subsurface material. In this study, we employed a Wenner array. The Wenner array measures subsurface changes in resistivity by moving an equally spaced pair of potential and current electrodes down the spread. A known electrical current is injected into the subsurface and the potential difference between two receivers is measured. Ohm's Law is used to calculate resistance from the current and potential difference data. The resistance, combined with a known electrode geometry, allows the instrument to convert the data to apparent resistivity.

The apparent resistivity data is then imported into AGI's 2D Earth Imager software for post-processing and inversion. The field data is debugged by removing any noisy data. The model parameters are optimized to produce the best possible inversion (Appendix A). The software then utilizes finite element modeling techniques (forward modeling) to create an inversion of the subsurface resistivity structure that is based on the apparent resistivity field data. The goal of the inversion is to create a model of the resistivity structure of the field site as it would have had existed to generate the observed field data. Each time the model iterates, it produces an inverted section of subsurface resistivity and a pseudo-section of calculated apparent resistivity. The calculated apparent resistivity pseudo-section is compared to the field data, an error is assigned to the iteration, and if the error criterion is not met, the model continues to iterate. The final product is an inverted section of subsurface resistivity whose calculated apparent resistivity pseudo-section closely resembles that of the field data. The surveyed patterns of subsurface electrical resistivity were then correlated to pore-water salinity by comparing resistivity to groundwater salinity sampling results (Section 3.3).

Plots showing percent difference in resistivity between surveys were also created to better visualize the location of large changes in resistivity. This was done by exporting the x- and y-coordinates for each node in the inverted resistivity section and its associated resistivity value. This data was exported for each of the four surveys. The percent difference in resistivity was then calculated at each node across the sections from two consecutive surveys. The percent difference values were assigned to the appropriate node and plotted in a contour plot.

3.3 Salinity Sampling

Groundwater salinity samples were collected from each monitoring well along the northwestern portion of Transect D to aid in the interpretation of the results from the electrical resistivity surveys. Salinity samples were collected on May 31, 2012, August 1, 2012, January 11, 2013, and May 23, 2013 from monitoring wells nests D21, D31, D51, D57, D76 and D89. The monitoring wells were purged of at least three well volumes of water using a Solinst peristaltic pump. After purging the wells, a small amount of groundwater was pumped into a rinsed plastic container and analyzed for salinity with a calibrated YSI EC300 probe. The probe was not allowed to come into contact with the sides of the sampling container while the measurement was being made, since this causes erroneous measurements to be reported.

3.4 Mean Water Level

Verified historical tidal data from the Charleston, SC (station # 8665530) harbor were obtained from the NOAA website at http://tidesandcurrents.noaa.gov for the years 1994 to 1996 and 2012 to 2013. The data reports water levels at one hour time intervals, referenced to MSL. This data was used to calculate a 29-day running average of MWL.

CHAPTER 4
RESULTS

4.1 Volumetric Flux and Net Flux

The calculated monthly average volumetric flux between Crabhaul Creek and monitoring wells D76, D89, and D117 vary in magnitude but all display an inverse relationship to the position of MWL (Figure 4.1, Figure 4.2, and Figure 4.3, respectively). The volumetric flux values range from 0.83 to 4.83 m^3d^{-1}. The inverse relationship between volumetric flux and MWL is evident in the period of record for each monitoring well nest. Seasonal highs in the position of MWL lead to decreased volumetric flux magnitudes while seasonal lows in the position of MWL lead to increased volumetric flux magnitudes. As the position of MWL transitions from a trough to a peak (e.g. Figure 4.1 between mid-June and mid-September), the volumetric flux responds by decreasing gradually from 1.36 to 1.08 m^3d^{-1}. Volumetric flux in these three locations is primarily controlled by the position of MWL. Table 4-1 statistically summarizes the results of the calculations and observations made at each well nest for the period of record.

Table 4.1 Volumetric flux statistics for periods of record

Well ID	Average Flux (m^3d^{-1})	Standard Deviation (m^3d^{-1})	Max Flux (m^3d^{-1})	Min Flux (m^3d^{-1})	Average Annual MWL	Period of Record
D76	1.22	0.1	1.36	1.05	0.0086	3/94-11/94
D89	4.01	0.38	4.83	3.50	0.0086	3/94-5/95
D117	0.98	0.1	1.09	0.83	0.0276	6/95-1/96

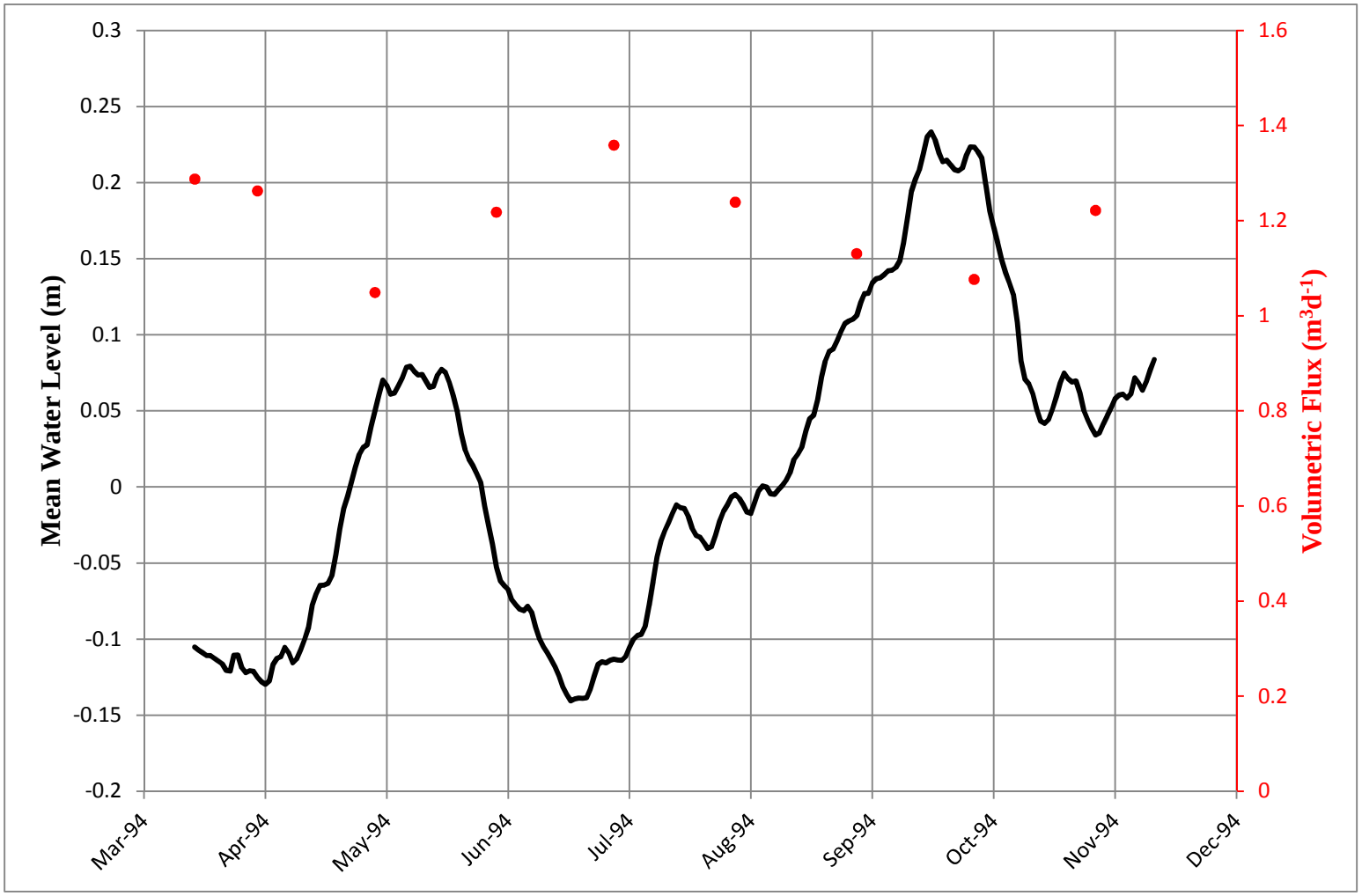

Figure 4.1 Volumetric flux at D76 (dots) and MWL (solid line) between March 1994 and November 1994.

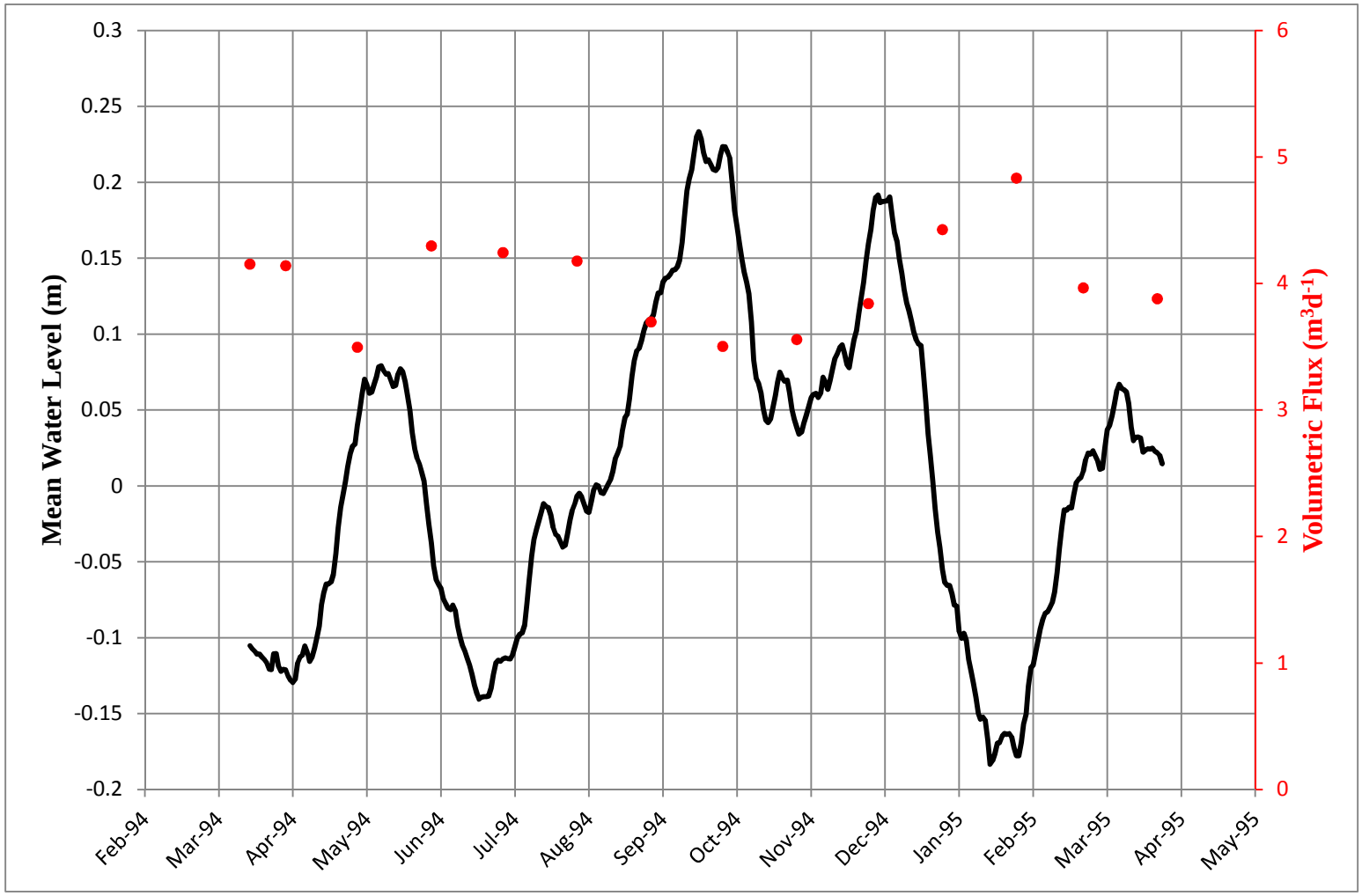

Figure 4.2 Volumetric flux at D89 (dots) and MWL (solid line) between March 1994 and April 1995.

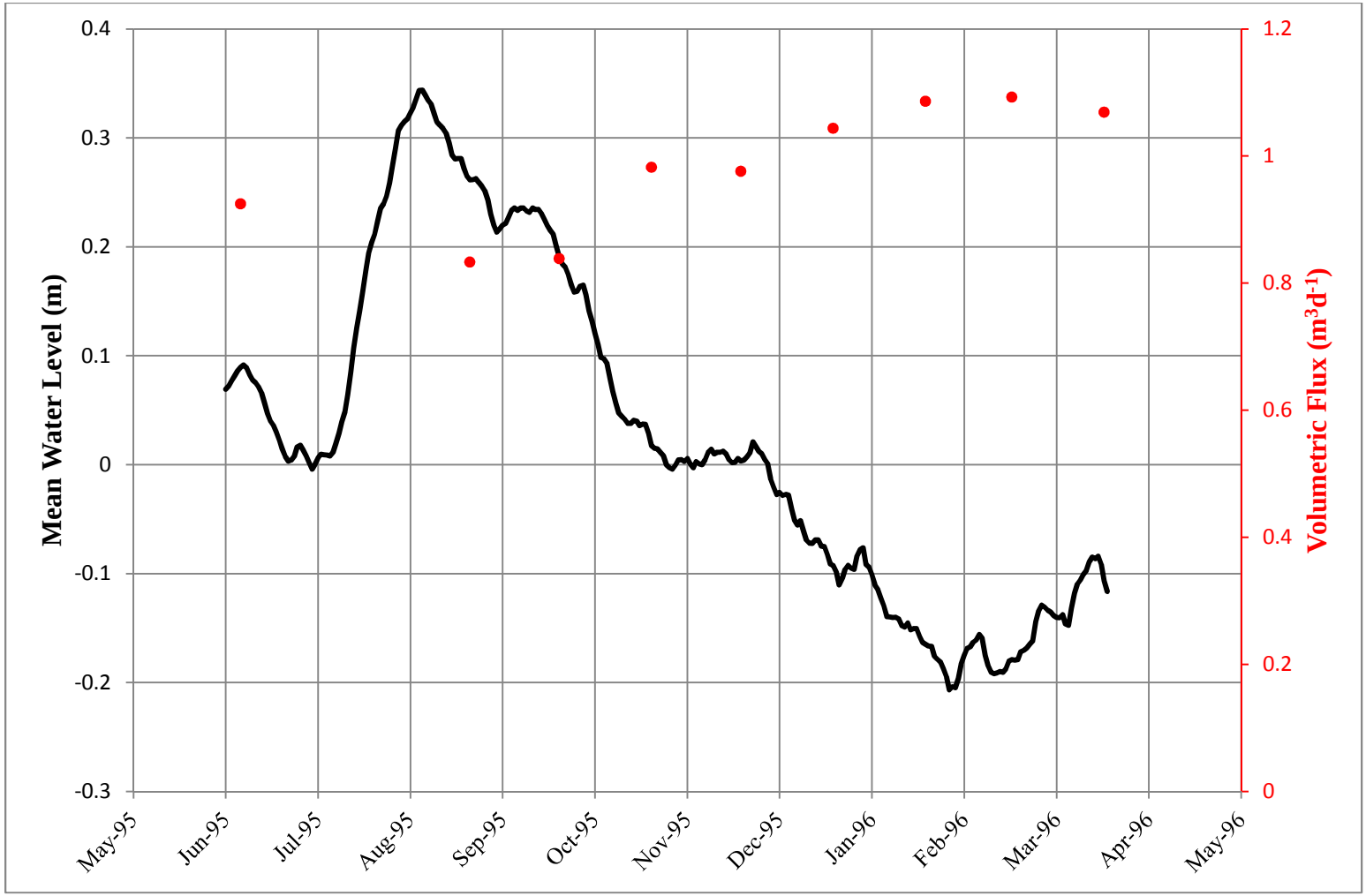

Figure 4.3 Volumetric flux at D117 (dots) and MWL (solid line) between June 1995 and April 1996.

The calculated monthly average volumetric flux values in the high-marsh at D51 range from 2.16 to 8.28 m^3d^{-1} and do not display the same inverse relationship to the position of MWL that is seen in the mid and low-lying marsh wells (Figure 4.4). Here, volumetric flux is controlled by precipitation, tidal amplitude, and MWL. This site is closer than D76 to the terrestrial watershed that exists in the forested upland. The hydraulic head records from 0.6 meters bgs and 3.6 meters bgs exhibit two unique hydraulic head signatures. The shallow well (0.6 meters bgs) generally has lower hydraulic head values than the deeper well (3.6 meters bgs) in the same location. The shallow well is also more responsive to the position of MWL and monthly tidal cycles. This is particularly clear on August 6, 1994, when hydraulic head rises sharply during inundating high tides. The deeper well is sensitive to precipitation events, and spikes in the hydraulic head record correlate well with large precipitation events. Rainfall causes rapid increases in the hydraulic head in the deeper part of the confined aquifer, followed by a gradual decrease. The frequency of precipitation events determines the hydraulic head in the deep well. The interaction of these factors control whether or not groundwater is discharging or seawater was infiltrating (Figure 4.5).

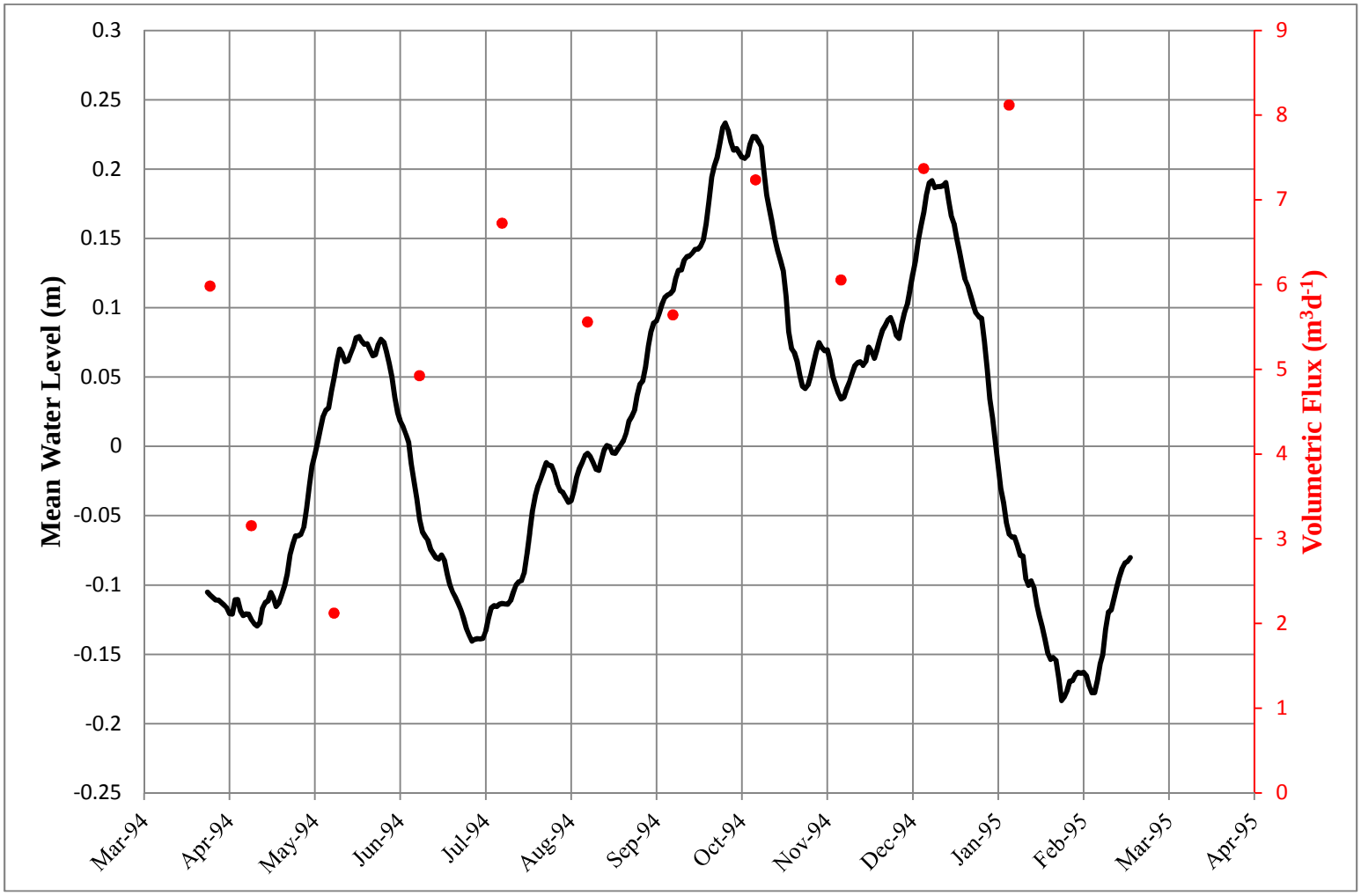

Figure 4.4 Volumetric flux at D51 (dots) and MWL (solid line) between March 1994 and April 1995.

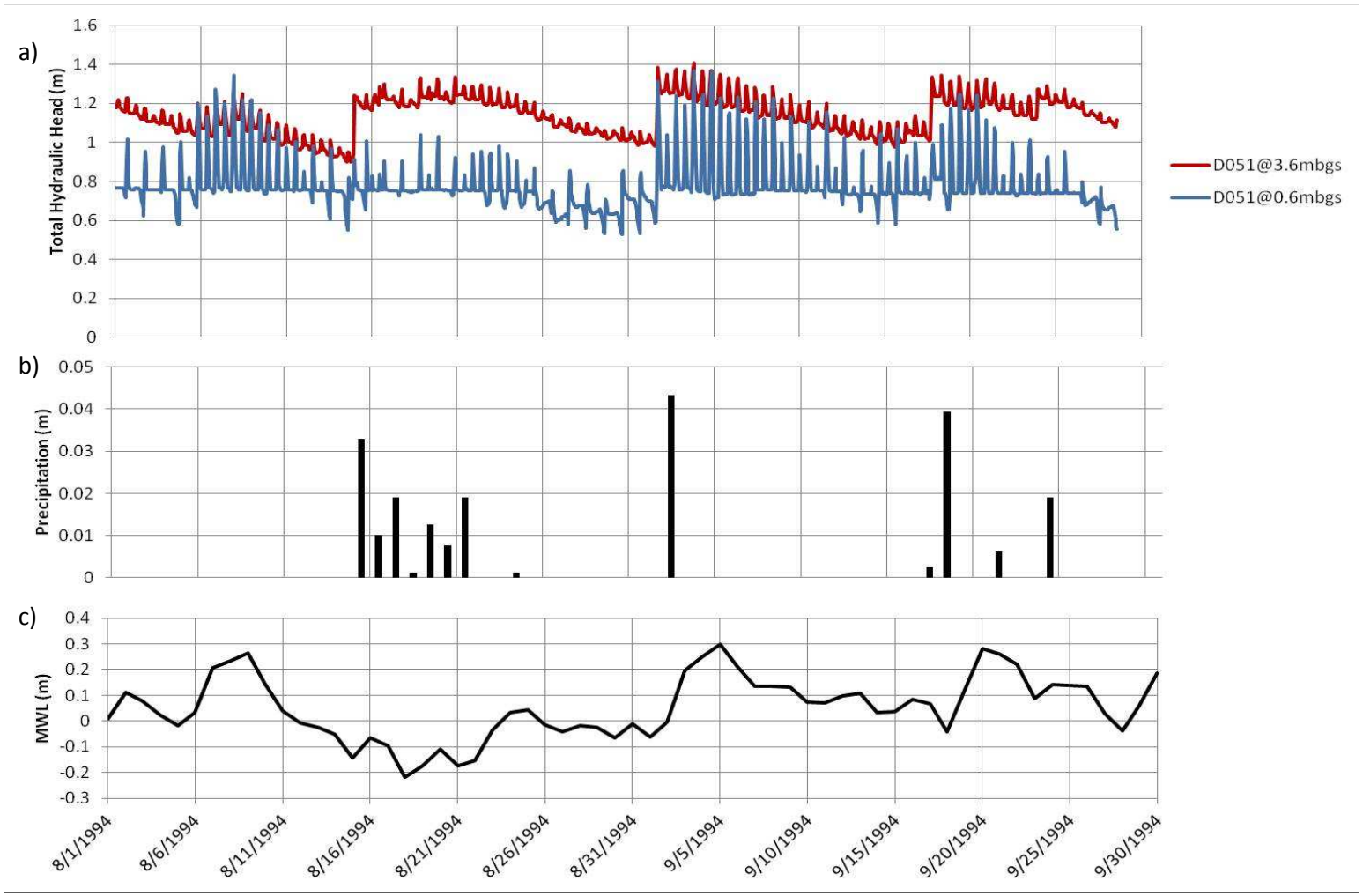

Figure 4.5 a) Hydraulic head record of D51 at 0.6 and 3.6 meters bgs. b) Precipitation record for North Inlet. c) 15-day running average of MWL

The difference between total discharge and net flux represents the total recharge that occurs along the surface of the Crabhaul Creek bank and increases with increasing tidal amplitude (Figure 4.6). During tidal cycles that had small amplitudes (0.44 m-0.56 m), very little recharge occurred. As tidal amplitude increased above 0.56 meters, total recharge became greater. Total recharge continued to increase with each increase in tidal amplitude from 0.56 meters to the maximum amplitude of 1.19 meters. The positive correlation of total recharge and total discharge to tidal amplitude is evident for each month in the D89 period of record.

A graph of total recharge plotted against the elevation of high tide (Figure 4.7) shows a positive correlation between the two data sets. Increases in the elevation of high tide drive increases in recharge magnitude. The plot also shows that a threshold exists, so that certain high tide elevations must be met to produce certain recharge magnitudes. For example, in order to achieve a total recharge of 0.5 meters per tidal cycle, the elevation of the high tide must be 0.76 meters or greater.

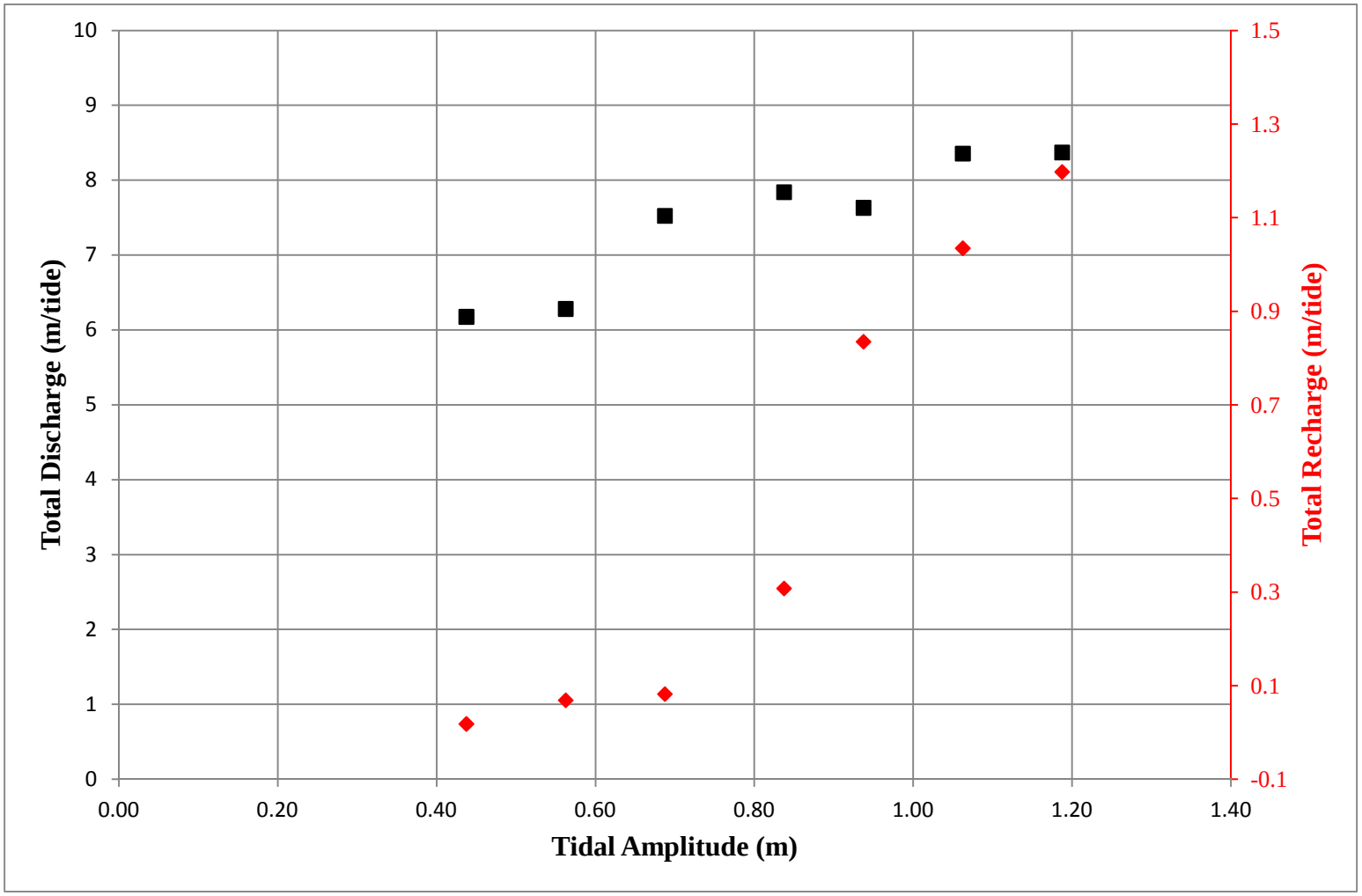

Figure 4.6 Total discharge and total recharge response to tidal amplitude in D89 (January 1995).

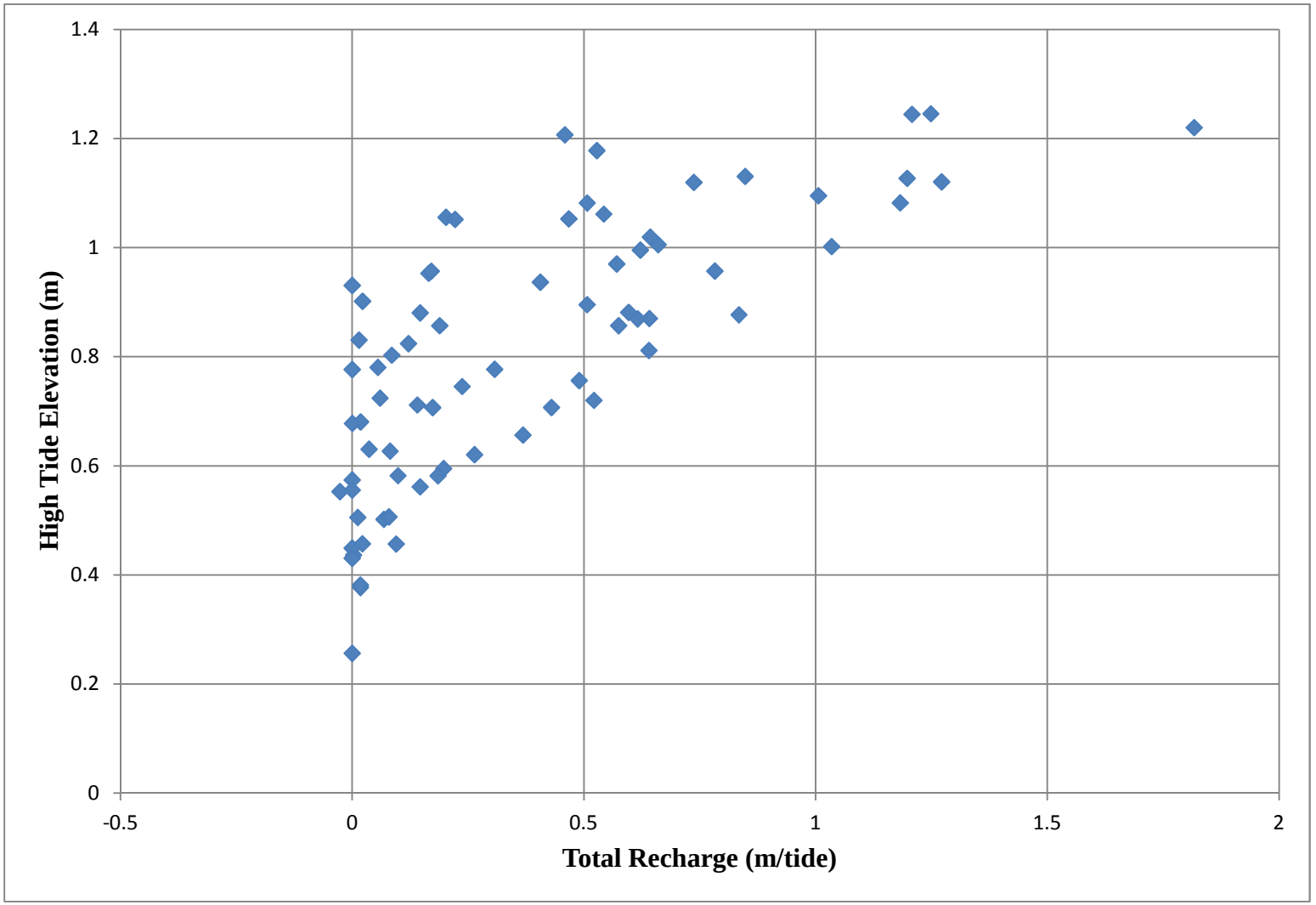

Figure 4.7 Elevation of high tide versus total recharge in D89 (April 1994 to April 1995)

4.2 Electrical Resistivity

All electrical resistivity surveys show two distinct zones (Figure 4.8). A zone of low resistivity extends from 21 meters to 94 meters relative to the NW end of Transect D. This zone extends from the surface to a maximum depth of 5 meters bgs. Resistivity values in this zone ranged from 28.4 to 1.4 Ohm-m and were indicative of marsh mud saturated by saline to brackish pore-water. A zone of higher resistivity originates in the forested upland and extends into the subsurface marsh beneath the confining clay unit and reaches a maximum depth of 20 meters bgs. The resistivity values in this zone range from 6.4 to 40 Ohm-m, which we interpret to represent sand saturated with brackish to fresh pore-water.

The plots of percent difference in resistivity show variability both zones throughout the course of the year (Figure 4.9). Between June 30, 2012 and August 1, 2012, there is an increase in resistivity throughout the shallow zone with the exception of an area between D45 and D50 that experienced a decrease in resistivity. The deeper zone exhibited an increase in resistivity between D15 and D55 but a decrease in resistivity from D55 to D89. Between August 1, 2012 and January 11, 2012, there was a general increase in resistivity in the shallow and deep zones. There were decreases in resistivity observed in the shallow zone between D85 and D105 and between D10 and D30 in the deeper zone. The percent difference plot between January 11, 2013 and May 22, 2013 displayed a general increase in resistivity in the shallow subsurface except for a decrease exhibited between D95 and D105. The deeper zone depicts an increase in resistivity between D10 and D30 but decreases between D25 and D50 and D70 and D100.

Each of the resistivity surveys was supplemented with in-situ salinity samples. The salinity samples were collected from monitoring wells along Transect D that were screened at a depth of approximately three meters bgs. The results were compared to the corresponding electrical resistivity surveys (Figure 4.10). The standard deviation of the resistivity and salinity data were calculated for each of the sampling dates (Table 4.2). Data misfit cross-plots and data misfit pseudo-sections were generated and are included as Appendix B. The resistivity results from each of the surveys show a steep decrease in resistivity between the forested upland at D21 (average resistivity equals16.7 Ohm-m) and the high marsh at D40 (average resistivity equals 3.5 Ohm-m). The resistivity values then level out at values ranging from 1.4 to 4.2 Ohm-m between the high marsh at D40 and the low-lying marsh at D89. The salinity samples show more variability between sampling events but generally salinity decreases from the upland at D21 to the high marsh at D40, then increases between D40 and Crabhaul Creek at D89. The maximum well depth along Transect D is 3.6 meters bgs, so it was not possible to obtain in-situ samples from below the confining unit.

Table 4.2 Statistical analysis of resistivity and salinity results.

Sampling Date	6/30/2012	8/1/2012	1/11/2013	5/22/2013
Resistivity Mean (Ohm-m)	4.97	4.47	4.86	7.46
Resistivity Standard Deviation (Ohm-m)	4.42	4.16	2.98	9.35
Salinity Mean (ppt)	8.57	5.42	6.43	5.43
Salinity Standard Deviation (ppt)	4.86	4.44	4.68	5.07

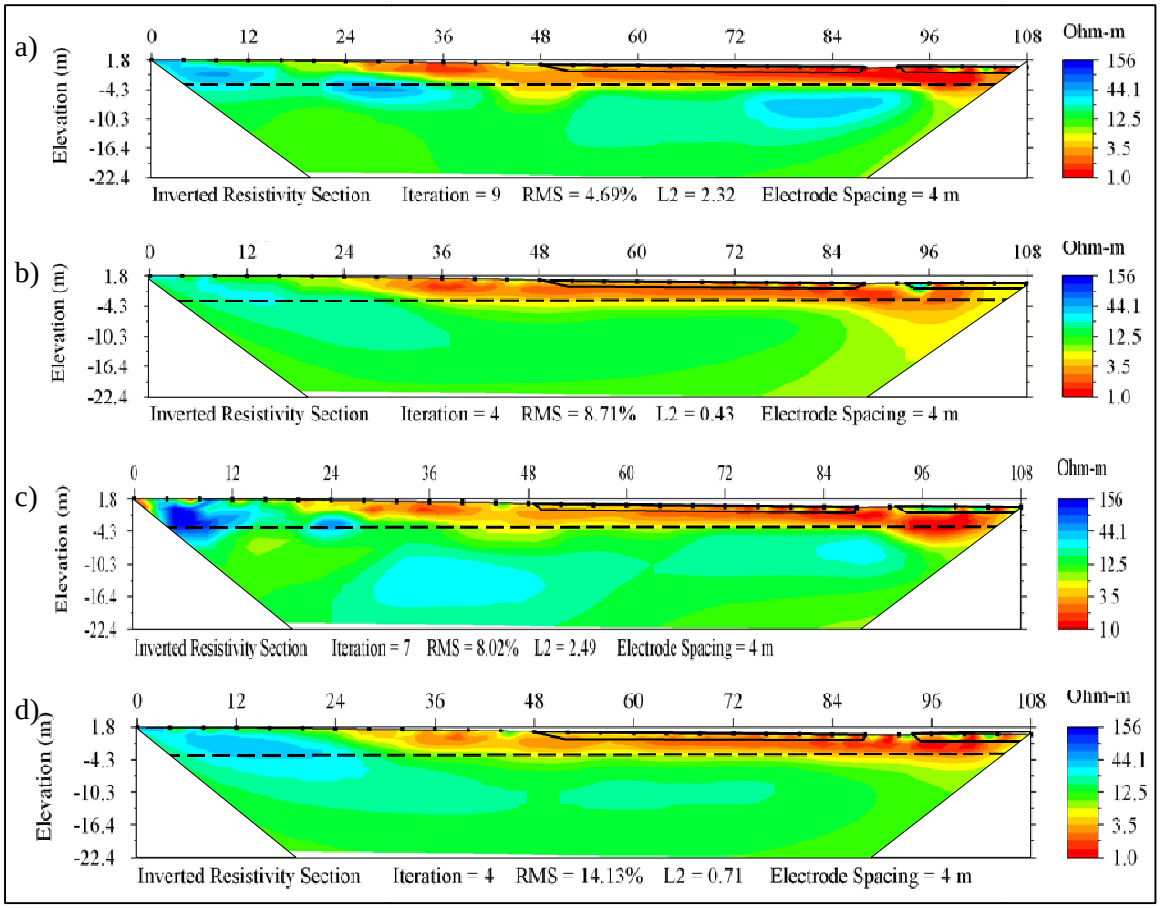

Figure 4.8 Electrical resistivity inversions from a) June 30, 2012, b) August 1, 2012, c) January11, 2013, and d) May 22, 2013. Dashed lines represent the clay unit. Solid lines represent mud layers.

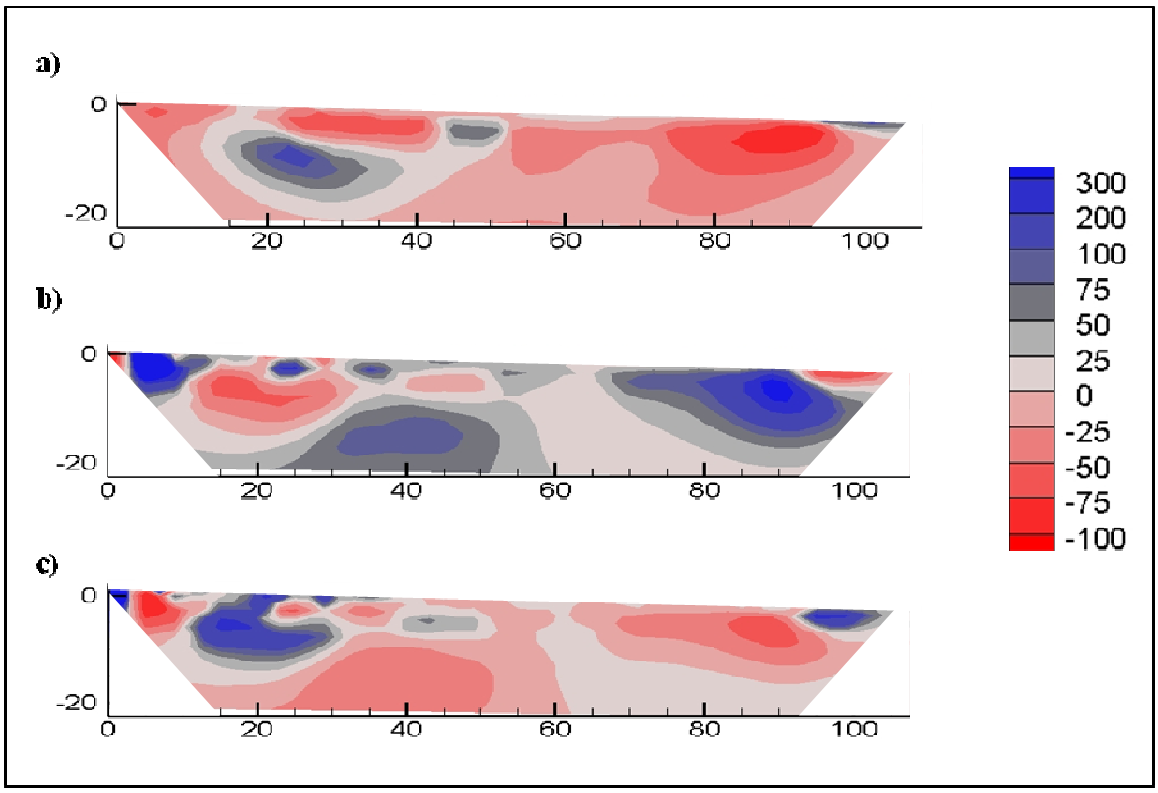

Figure 4.9 Percent difference plots (%) between a) June and August 2012 b) August 2012 and January 2013 and c) January and May 2013.

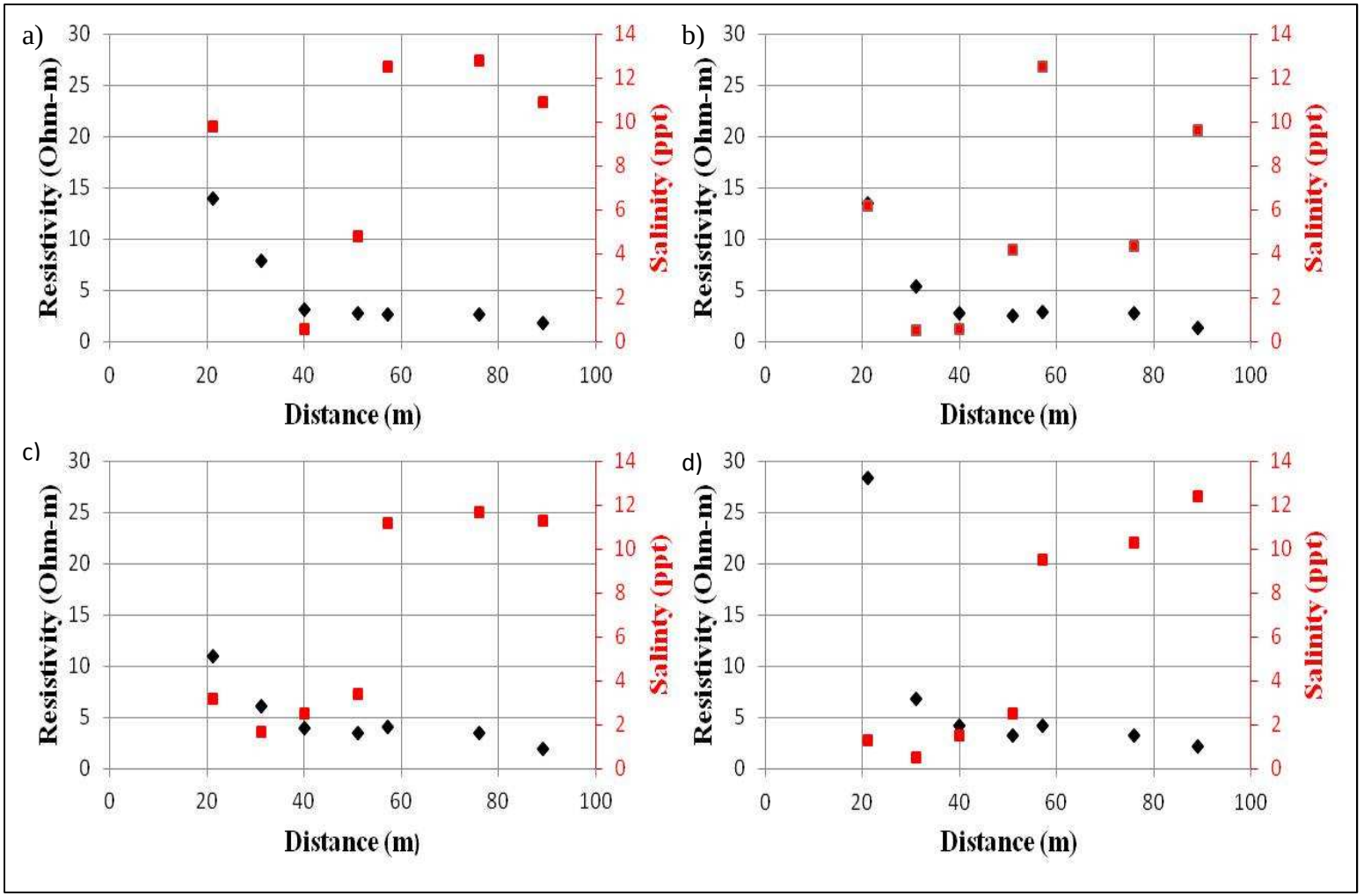

Figure 4.10 Salinity and resistivity plotted against distance along Transect D at a depth of 3 meters for a) June 30, 2012 b) August 1, 2012 c) January 11, 2013, and d) May 22, 2013

CHAPTER 5
DISCUSSION

The results from this study show that groundwater discharge and recharge along Transect D are controlled by a combination of MWL, tidal amplitude, and precipitation. The factors that control advective groundwater flow transition from the forested upland to Crabhaul Creek. In the low marsh adjacent to Crabhaul Creek and in the mid-marsh at D76, the magnitude of tidally influenced groundwater discharge and recharge is predominately controlled by the position of MWL. In the high-marsh at D51, vertical groundwater flow is controlled by a complex interaction between MWL, tidal amplitude, and precipitation.

The elevation of MWL can vary by as much as 0.5 meters over the course of a year and strongly affects the magnitude of groundwater discharge in the mid- and low marsh. Groundwater discharge displays an inverse relationship with the position of MWL in the mid and low-lying marsh. This means that periods of low MWL produce higher rates of groundwater discharge and higher MWL produces lower rates of groundwater discharge. The range of tidal amplitude values is fairly constant throughout the year in the North Inlet, but seasonal changes in MWL influence these tidal amplitudes by increasing or decreasing their vertical reach across the marsh platform. This in turn affects the area of the marsh platform that is inundated during high tides, the area of the creek bank that is exposed during low tide, and the hydraulic gradient between the subsurface marsh and Crabhaul Creek. During periods of high MWL, large areas of the

marsh platform are inundated at high tide but a small area of the creek bank is exposed at low tide. During periods of low MWL, smaller areas of the marsh platform are inundated but more of the creek bank is exposed at low tide. More groundwater is discharged through the creek bank at periods of low tide and low MWL because there is a larger hydraulic gradient between the marsh groundwater and the surface water in Crabhaul Creek. At periods of high MWL, there is a smaller hydraulic gradient and lower groundwater discharge magnitudes. These results are consistent with the results of Wilson and Morris (2012), who suggested an inverse relationship between MWL and groundwater discharge. It appears that this relationship holds for forest-marsh boundaries as well as for salt marsh islands.

Groundwater flow in the high marsh along Transect D is influenced by the terrestrial watershed to the northwest, precipitation events, MWL position, and tidal amplitude. The hydraulic head in the 3.6 meters bgs well at the D51 location is influenced by precipitation and tidal cycles. The hydraulic head variations caused by the precipitation events are much greater than the variations caused by tidal cycles. The shallow well at D51, which is screened at 0.6 meters bgs, is much more responsive to daily and monthly tidal cycles and is not influenced by precipitation. The ranges in hydraulic head associated with the tidal cycles are much larger in the shallow well than in the deep well. The increases and decreases in hydraulic head in this well correspond nicely to the fluctuations in MWL due to spring and neap tidal cycles. The interaction between these factors determines if discharge or recharge is occurring between the two screened intervals. For example, consider a large precipitation even that occurs during a neap tidal cycle during a period of low MWL. There would be a high hydraulic head in

the deep interval driven by the rain event and a low hydraulic head in the shallow well due to the reduced amplitudes associated with the neap tidal cycles and the low position MWL. This would create a discharge zone in the high marsh with a magnitude proportional to the difference in hydraulic head between the deep and shallow wells.

Volumetric flux values calculated for the mid-marsh on the northwestern side of the transect (D76) are 23 % larger than discharge calculated for the mid-marsh on the southeastern side of the transect (D117). This was a surprising result, as we hypothesized that groundwater discharge would be significantly greater on the northwestern side of the transect due to the fact that a 75 square kilometer terrestrial watershed exists directly up-gradient. Based on these results, the presence of a large freshwater lens in the upland does not seem to significantly impact discharge. It appears that discharge from the large upland bypasses the marsh, discharging at D51 or traveling through the fresher aquifer below the confining unit.

Volumetric fluxes through the creek bank were converted to a flux per unit area of the marsh via the creek density so that our fluxes could be compared to other estimates. Creek density is the ratio of the length of creek bank to the area of marsh. The creek density in the Crabhaul Creek Basin is 0.01 m^{-1}, which is the same as the creek density calculated for North Inlet by Novakowski et al (2004). We report volumetric flux and flux per unit area to be consistent with both the groundwater and salt marsh literature. The magnitude of groundwater discharge that we calculated based on data from D89 and converted using the creek density term is slightly higher than previous values that have been calculated for the North Inlet Basin (Table 5-2). The minimum value calculated in this study was 36.01 $Lm^{-2}d^{-1}$. The maximum value calculated in this study was 49.77

$Lm^{-2}d^{-1}$. Based on previous studies, a maximum value of 40 $Lm^{-2}d^{-1}$ was calculated for North Inlet by Krest et al. (2000) using radium isotope groundwater tracers. The larger values can be attributed to the continuous nature of our monitoring and the seasonal variations in groundwater discharge that emerged. The former studies from North Inlet only achieved temporal "snap shots" of groundwater discharge which cannot be considered representative of the system due to the variable tendencies that we observed. Krest et al. (2000) also noted that significant groundwater discharged through the creek bottom, which raised the question of whether the discharging groundwater originated in the marsh or in a deeper aquifer. Our results suggest that tidal fluctuations in the marsh are adequate to explain the fluxes observed by Krest et al (2000).

Table 5.1 Results of current and former groundwater studies in North Inlet

Study Author(s)	Location	Method	Discharge ($Lm^{-2}d^{-1}$)
Whiting and Childers (1989)	North Inlet, SC	Seepage meter	7.8-28
Morris (1995)	North Inlet, SC	Salt and water balance	9.4-16.6
Krest et al (2000)	North Inlet, SC	Radium tracers	20-40
Wilson and Gardner (2006)	North Inlet, SC	Numerical simulations	10-14
This study	North Inlet, SC	Darcy flux calculations	36.01-49.77

Groundwater recharge also occurs at the creek bank along Transect D and displays a positive correlation with high tide elevation. At lower high tide elevations, the total recharge that occurs is non-existent or minimal. This is due to the fact that the height of the surface water in the creek is not large enough to reverse the hydraulic gradient. Increases in the elevation of high tide are a result of both larger tidal amplitudes and

higher MWL. As the elevation of high tide gradually increases from 0.3 meters to 1.2 meters, more and more seawater begins to infiltrate at the creek bank. Higher MWL combined with larger tidal amplitudes create surface water heights in the creek capable of reversing the component of flow during the peaks of each tidal cycle. This leads to substantial groundwater exchange along the creek bank.

We hypothesized that salinity in the shallow subsurface (up to four meters bgs) would display seasonal variations that were related to seasonal variations in discharge, but the electrical resistivity surveys and in-situ salinity sampling data contradict this hypothesis. Tobias et al. (2001) suggested that "groundwater mediated" flushing associated with seasonal variations in groundwater discharge flushed the subsurface marsh of salts and nutrients. Carter et al. (2007) also showed that a freshwater/saltwater interface existed along Transect C in North Inlet and that the lateral extent of this interface migrated on a monthly timescale. Our results suggest that the saline to brackish zone that exists in the shallow subsurface experiences temporal and spatial variability that is not easily correlated to precipitation or the position of MWL (Figure 5.1).

Variation in electrical resistivity was much more apparent in the deeper zone between the clay confining unit and approximately 20 meters bgs. The percent difference plot presented in Figure 4.9 shows two areas in the deep subsurface that alternate between increasing and decreasing resistivity over the course of a year. The first area is located at a depth of five to 15 meters bgs and laterally between 10 and 30 meters from the NW end of Transect D. The second area is located between five and 15 meters bgs and laterally between 65 and 100 meters from the NW end of Transect D. These alterations in resistivity do not correlate with precipitation events or the position of

MWL. It is clear that lithologic changes do not occur on this time scale, so the resistivity variations must be due to groundwater processes. We believe that the deeper, higher resistivity zone (freshwater zone) is hydraulically disconnected from the upper saline to brackish zone and could be part of a larger flow path that connects the forested upland to some discharge point to the southeast of Transect D. The relationship between rainfall and changes in resistivity in the deeper zone needs further investigation.

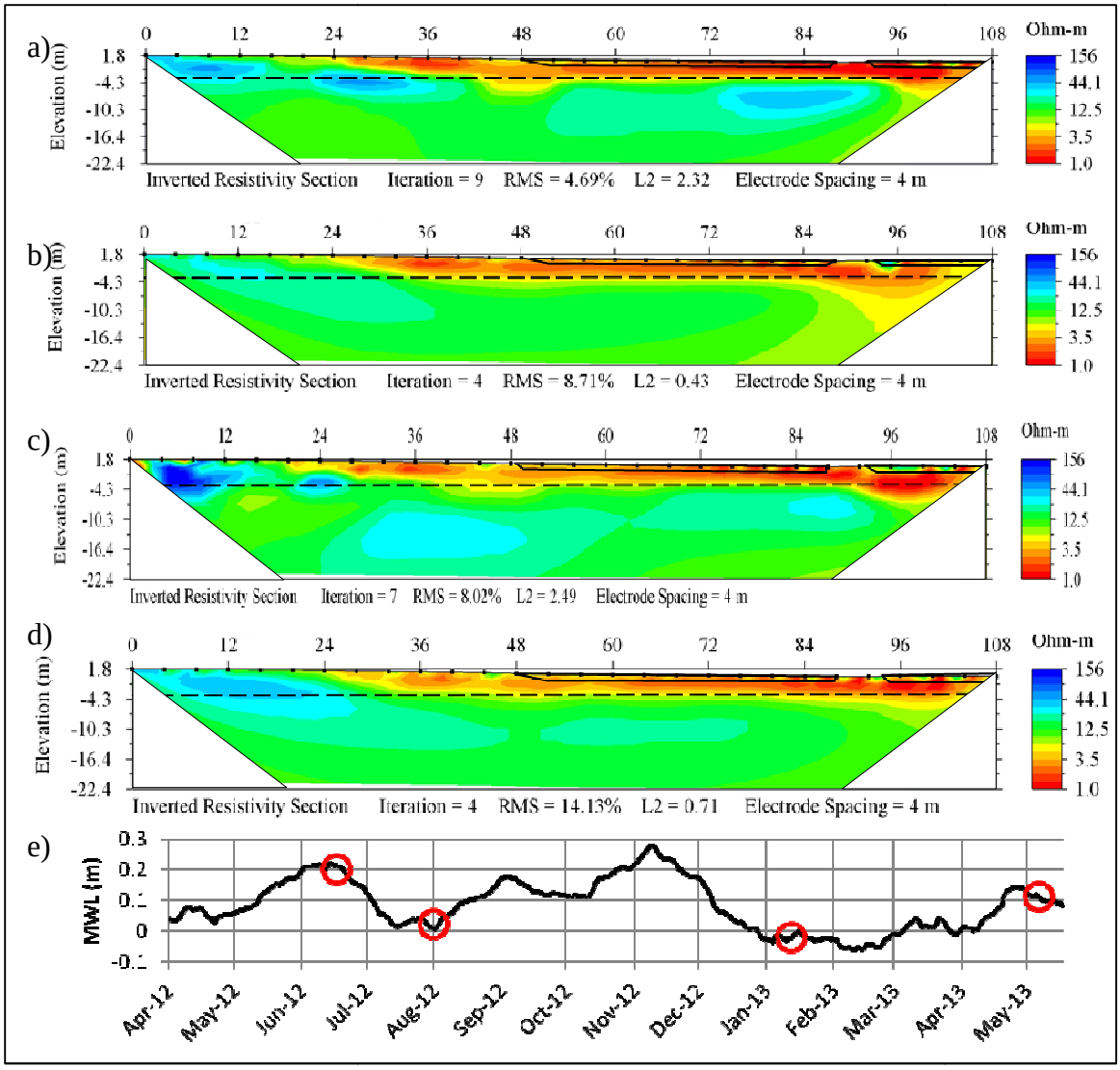

Figure 5.1 Electrical resistivity surveys a) June 30, 2012, b) August 1, 2012, c) January11, 2013, and d) May 22, 2013 and e) 29-day running average of MWL position.

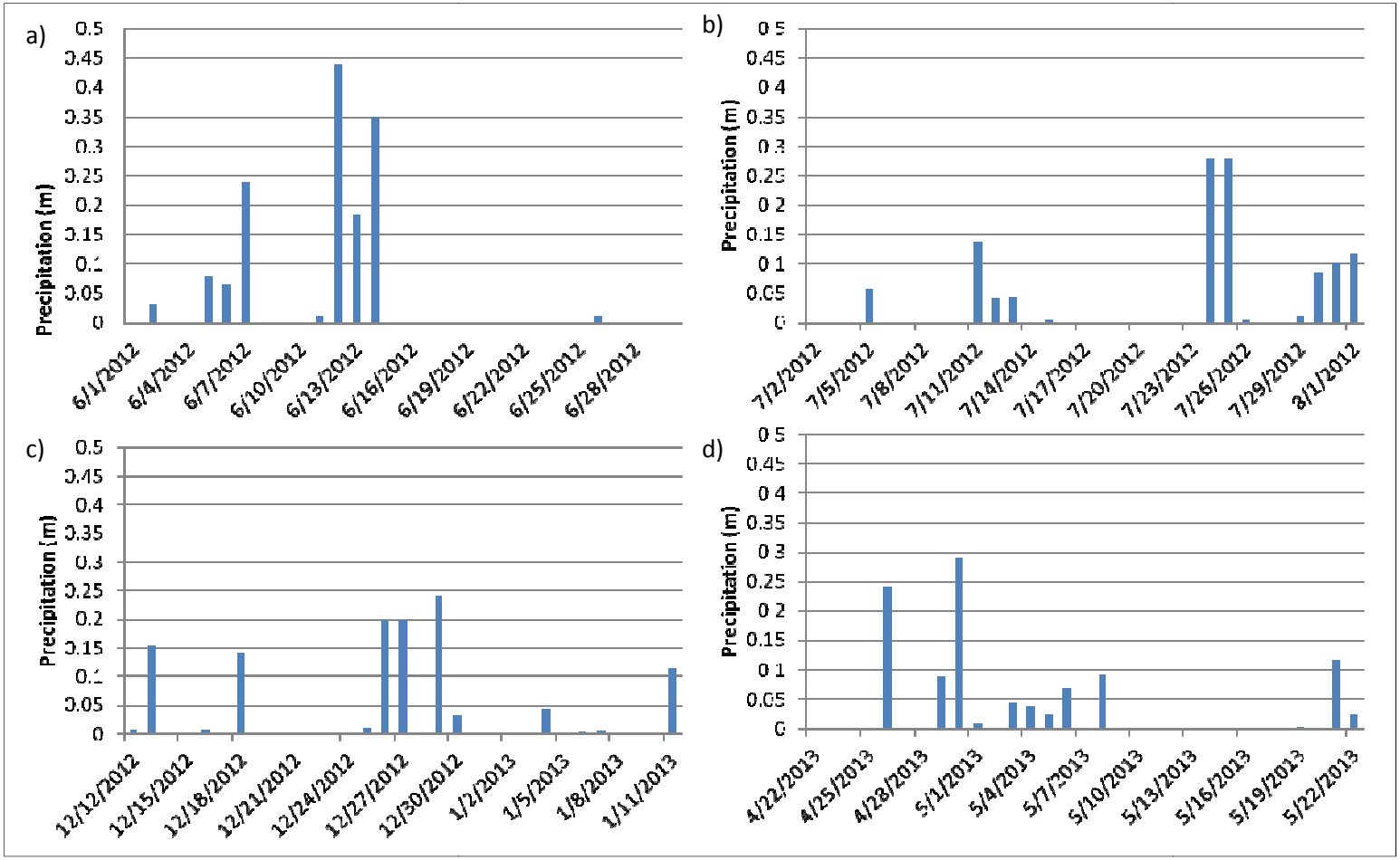

Figure 5.2 Daily precipitation totals for a) June 1 to 30, 2012 b) July 2 to August 1, 2012 c) December 12 to 27, 2012 d) April 23 to May 7, 2013.

CHAPTER 6
CONCLUSION

This study quantitatively shows that discharge from a fringing marsh is variable on a seasonal basis and the factors that control the flow of groundwater through the marsh are determined by the location within the system. Groundwater discharge at the low-lying and mid-marsh locations is predominantly controlled by the elevation of MWL. There is an inverse relationship that exists at these locations between the position of MWL and the magnitude of groundwater discharge. In the high-marsh, groundwater discharge is influenced by MWL, tidal amplitude, and precipitation. The interactions of these factors determine whether groundwater discharges or recharges and the magnitude of this flow.

There are two primary zones that occur in the subsurface along Transect D which are separated by a confining clay unit. The top zone has a pore-water salinity that is saline to brackish. In this zone, freshwater that makes it past the high-marsh location is mixed with seawater that infiltrates through the creek bank and the marsh mud. The brackish and saline water is transported slowly through the subsurface and eventually discharges at the creek bank of Crabhaul Creek. The deeper zone displays resistivity signatures indicative of freshwater. There are two flow paths that the freshwater in the upland can take. First, it can be transported above the confining clay unit, where it is mixed and discharged in the high marsh or at the creek bank. The second is that it can

flow under the confining clay unit where it is isolated from the saline water above and discharged further to the east.

The variable magnitude of groundwater discharge along the transect and the mixing that occurs in the upper zone are important when considering nutrient export. Groundwater must have a salinity concentration of greater than ten ppt to transport nutrients. This implies that along Transect D all of the nutrients are being exported from the shallow, saline to brackish zone. Nutrient export is proportional to groundwater discharge. The seasonal variation that we see in discharge can potentially introduce pulses of nutrient enriched groundwater into the adjacent coastal water. Also, long term sea level rise that occurs at a rate that is faster than sediment accretion would decrease groundwater discharge, nutrient export, and estuarine fertility.

REFERENCES

Carr, P.A. and V.D. Kamp, Determining aquifer characteristics by the tidal method, *Water Resources Research*, 5(5), 1023-1031, 1969

Carter, E.S., S.M. White, and A.M. Wilson, Variation in groundwater salinity in a tidal salt marsh basin, North Inlet Estuary, South Carolina, *Estuarine, Coastal and Shelf Science*, 76, 543-552, 2008.

Dame, R.F., and L.R. Gardner, Nutrient processing and the development of tidal creek ecosystems, *Marine Chemistry*, 43, 175-183, 1993.

De Meneses, J.G.A., Modeling the fresh water inflow to the Pettaquamscutt River. Ph.D. thesis, University of Rhode Island.

Gardner, L.R., and D.E. Porter, Stratigraphy and geologic history of a southeastern salt marsh basin, North Inlet, South Carolina, USA, *Wetlands Ecology and Management*, 9, 371-385, 2001.

Harvey, J.W. and W.K. Nuttle, Fluxes of water and solute in a coastal wetland sediment. *Journal of Hydrology*, 164, 109-125, 1995.

Kelly, R.P., and S.B. Moran, Seasonal changes in groundwater input to a well-mixed estuary estimated using radium isotopes and implications for coastal nutrient budgets, *Limnology and Oceanography*, 47(6), 1796-1807, 2002.

Keenan, R.S., An investigation of the dynamics of groundwater flow and salinity distribution along a forest-marsh transect. Ph.D. thesis, Columbia: University of South Carolina

Krest, J.M., W.S. Moore, L.R. Gardner, and J.T. Morris, Marsh nutrient export supplied by groundwater discharge, *Global Biogeochemical Cycles*, 14(1), 167-176, 2000.

Morris, J.T., The mass balance of salt and water in intertidal sediments: results from North Inlet, South Carolina, *Estuaries*, 18(4), 556-567, 1995.

Nixon, S.W., Between coastal marshes and coastal waters-a review of twenty years of speculation and research on the role of salt marshes in estuarine productivity and water chemistry, Estuarine and Wetland Processes, 437-525, 1980.

Novakowski, K.I., R. Torres, L.R. Gardner, and G. Voulgaris, Geomorphic analysis of tidal creek networks, *Water Resources Res.*, 40, W05401, doi:10.1029/2003WR002722, 2004.

Reilly, T.E., and A.S. Goodman, Quantitative analysis of saltwater-freshwater relationships in groundwater systems-a historical perspective, Journal of Hydrology, 80, 125-160, 1985.

Thibodeau, P.M., Groundwater flow dynamics across the forest-salt marsh interface: North Inlet, SC. Ph.D. thesis, Columbia: University of South Carolina

Tobias, C.R., J.W. Harvey, and I.C. Anderson, Quantifying groundwater discharge through fringing wetlands to estuaries: seasonal variability, methods comparison, and implications for wetland-estuary exchange, *Limnology and Oceanography*, 46(3), 604-615, 2001.

U.S. Geological Survey, Water resources data reports for South Carolina, Columbia, SC, 1983-1993.

Whiting, G.J., and D.L. Childers, Subtidal advective water flux as a potentially important nutrient input to southeastern U.S.A. saltmarsh estuaries, *Estuarine Coastal Shelf Science*, 28(4), 417-431, 1989.

Wilson, A.M., and J.T. Morris, The influence of tidal forcing on groundwater flow and nutrient exchange in a salt marsh-dominated estuary, *Biogeochemistry*, 108, 27-38, 2012.

Wilson, A.M., and L.R. Gardner, Tidally driven groundwater flow and solute exchange in a marsh: numerical simulations, *Water Resources Research*, 42, W01405, doi:10.1029/2005WR004302, 2006.

APPENDIX A
ELECTRICAL RESISTIVITY PARAMETERS

June 30, 2012 Survey Parameters

Advanced Geosciences Inc. (AGI) Sting/SuperSting measured data (*.stg) Type: XYZ
A trimmed data set by AGI EarthImager 2D. Version: 2.4.0 (Build 617). Records: 279
Raw data file: C:\Documents and Settings\jpeurifoy\Desktop\Thesis Information\Research Data\Resistivity\6.30.12\TRAND1_Reversed\trial3\TRAND1_Reversed_trial3.stg
Terrain file: C:\Documents and Settings\jpeurifoy\Desktop\Thesis Information\Research Data\Resistivity\6.30.12\TRAND1\TranD12.trn

Number of Data = 279
Number of Electrodes = 28
Number of Surface Electrodes = 28
Number of IP Data = 0

Processing starts at 2012-09-13 12:30:13

;------ SETTINGS ------

Minimum Voltage (mv) = -1
Minimum V/I (ohm) = 0.0002
Minimum apparent resistivity (ohm-m) = 0.1
Maximum apparent resistivity (ohm-m) = 10000
Maximum repeat error (%) = 7
Maximum reciprocal error (%) = 10
Remove negative apparent resistivity in ERT data: Yes
Keep All Data (no data removal): No
Inversion Method: Smooth model inversion
Vertical axis: Positive Upward
Y Coordinate = Depth
Min electrode spacing X (m) = 0.003
Min electrode spacing Z (m) = 0.003
Forward Modeling Method: Finite element method
Forward system solver: Cholesky decomposition method
Boundary condition type: Dirichlet
Number cells or elements betwenn two electrodes = 2
Lower-layer-thickness / Upper-layer-thickness = 1.1
Depth of Inverted Model / Depth of Pseudosection = 1.1

Max number of iteration of nonlinear inversion = 10
Stop RMS error = 3%
Mininum error reduction between two iterations = 5%
Stop at Max number of iterations: Yes
Stop when RMS is small enough: No
Stop when RMS can not be reduced: No
Res Data reweighting: No
Use Reciprocal Error: No
Stop when L2 norm is small enough: No
Initial smoothness factor = 1000.0
Roughness conditioner = 0.2
Starting model: Avg AppRes.
Start halfspace resistivity = 7.08 ohm-m
Minimum resistivity = 1.0 ohm-m
Maximum resistivity = 100000.0 ohm-m
Number of elements combined horizontally = 1
Number of elements combined verically = 1
Vertical / Horizontal roughness ratio = 0.2
Estimated noise of resistivity data = 3%
Initial damping factor of resistivity = 1000.0
Starting iteration of quasi Newton method = 20
IP inversion method: No IP Inversion
Terrain mesh transform method: Damped transform.

;------ ELECTRODE LOCATIONS ------

Electrode	X	Y	Terrain_X	Terrain_Y
0,	0.000,	0.000,	0.000,	0.000
1,	4.000,	0.000,	4.000,	-0.029
2,	8.000,	0.000,	8.000,	-0.058
3,	12.000,	0.000,	12.000,	-0.087
4,	16.000,	0.000,	16.000,	-0.122
5,	20.000,	0.000,	20.000,	-0.188
6,	24.000,	0.000,	24.000,	-0.262
7,	28.000,	0.000,	28.000,	-0.341
8,	32.000,	0.000,	32.000,	-0.420
9,	36.000,	0.000,	36.000,	-0.499
10,	40.000,	0.000,	40.000,	-0.581
11,	44.000,	0.000,	44.000,	-0.692
12,	48.000,	0.000,	48.000,	-0.845
13,	52.000,	0.000,	52.000,	-1.023
14,	56.000,	0.000,	56.000,	-1.096
15,	60.000,	0.000,	60.000,	-1.157
16,	64.000,	0.000,	64.000,	-1.210
17,	68.000,	0.000,	68.000,	-1.262
18,	72.000,	0.000,	72.000,	-1.315

19,	76.000,	0.000,	76.000,	-1.367
20,	80.000,	0.000,	80.000,	-1.413
21,	84.000,	0.000,	84.000,	-1.457
22,	88.000,	0.000,	88.000,	-1.502
23,	92.000,	0.000,	92.000,	-1.454
24,	96.000,	0.000,	96.000,	-1.393
25,	100.000,	0.000,	100.000,	-1.347
26,	104.000,	0.000,	104.000,	-1.394
27,	108.000,	0.000,	108.000,	-1.440

August 1, 2012 Survey Parameters

Advanced Geosciences Inc. (AGI) Sting/SuperSting measured data (*.stg) Type: XYZ
A trimmed data set by AGI EarthImager 2D. Version: 2.4.0 (Build 617). Records: 292
Raw data file: C:\Documents and Settings\jpeurifoy\Desktop\Thesis Information\Research Data\Resistivity\8.1.12\4m MRT Poster 8.1.12\11TRAND_Reversed\trial3\11TRAND_Reversed_trial3.stg
Terrain file: C:\Documents and Settings\jpeurifoy\Desktop\Thesis Information\Research Data\Resistivity\8.1.12\4m MRT Poster 8.1.12\TranD12.trn

Number of Data = 292
Number of Electrodes = 28
Number of Surface Electrodes = 28
Number of IP Data = 0

Processing starts at 2013-09-23 10:33:07

;------ SETTINGS ------

Minimum Voltage (mv) = 1
Minimum V/I (ohm) = 0.0005
Minimum apparent resistivity (ohm-m) = 0.01
Maximum apparent resistivity (ohm-m) = 10000
Maximum repeat error (%) = 7
Maximum reciprocal error (%) = 10
Remove negative apparent resistivity in ERT data: Yes
Keep All Data (no data removal): No
Inversion Method: Smooth model inversion
Vertical axis: Positive Upward
Y Coordinate = Depth
Min electrode spacing X (m) = 0.003
Min electrode spacing Z (m) = 0.003
Forward Modeling Method: Finite element method
Forward system solver: Cholesky decomposition method
Boundary condition type: Dirichlet
Number cells or elements betwenn two electrodes = 2

Lower-layer-thickness / Upper-layer-thickness = 1.1
Depth of Inverted Model / Depth of Pseudosection = 1.1
Max number of iteration of nonlinear inversion = 15
Stop RMS error = 5%
Mininum error reduction between two iterations = 3%
Stop at Max number of iterations: No
Stop when RMS is small enough: No
Stop when RMS can not be reduced: No
Res Data reweighting: Yes
Use Reciprocal Error: No
Stop when L2 norm is small enough: Yes
Initial smoothness factor = 100
Roughness conditioner = 0.1
Starting model: Avg AppRes.
Start halfspace resistivity = 7.01 ohm-m
Minimum resistivity = 1.0 ohm-m
Maximum resistivity = 100000.0 ohm-m
Number of elements combined horizontally = 1
Number of elements combined verically = 1
Vertical / Horizontal roughness ratio = 0.2
Estimated noise of resistivity data = 5%
Initial damping factor of resistivity = 100
Starting iteration of quasi Newton method = 20
IP inversion method: No IP Inversion
Terrain mesh transform method: Damped transform.

;------ ELECTRODE LOCATIONS ------

Electrode	X	Y	Terrain_X	Terrain_Y
0,	0.000,	0.000,	0.000,	0.000
1,	4.000,	0.000,	4.000,	-0.029
2,	8.000,	0.000,	8.000,	-0.058
3,	12.000,	0.000,	12.000,	-0.087
4,	16.000,	0.000,	16.000,	-0.122
5,	20.000,	0.000,	20.000,	-0.188
6,	24.000,	0.000,	24.000,	-0.262
7,	28.000,	0.000,	28.000,	-0.341
8,	32.000,	0.000,	32.000,	-0.420
9,	36.000,	0.000,	36.000,	-0.499
10,	40.000,	0.000,	40.000,	-0.581
11,	44.000,	0.000,	44.000,	-0.692
12,	48.000,	0.000,	48.000,	-0.845
13,	52.000,	0.000,	52.000,	-1.023
14,	56.000,	0.000,	56.000,	-1.096
15,	60.000,	0.000,	60.000,	-1.157
16,	64.000,	0.000,	64.000,	-1.210

17,	68.000,	0.000,	68.000,	-1.262
18,	72.000,	0.000,	72.000,	-1.315
19,	76.000,	0.000,	76.000,	-1.367
20,	80.000,	0.000,	80.000,	-1.413
21,	84.000,	0.000,	84.000,	-1.457
22,	88.000,	0.000,	88.000,	-1.502
23,	92.000,	0.000,	92.000,	-1.454
24,	96.000,	0.000,	96.000,	-1.393
25,	100.000,	0.000,	100.000,	-1.347
26,	104.000,	0.000,	104.000,	-1.394
27,	108.000,	0.000,	108.000,	-1.440

January 11, 2013 Survey Parameters

Advanced Geosciences Inc. (AGI) Sting/SuperSting measured data (*.stg) Type: XYZ
A trimmed data set by AGI EarthImager 2D. Version: 2.4.0 (Build 617). Records: 301
Raw data file: C:\Documents and Settings\jpeurifoy\Desktop\Thesis Information\Research Data\Resistivity\1.11.13\4m MRT 1.11.13\110133_Reversed\trial1\110133_Reversed_trial1.stg
Terrain file: C:\Documents and Settings\jpeurifoy\Desktop\Thesis Information\Research Data\Resistivity\1.11.13\4m MRT 1.11.13\TRAND4m.trn

Number of Data = 301
Number of Electrodes = 28
Number of Surface Electrodes = 28
Number of IP Data = 0

Processing starts at 2013-05-29 13:48:55

;------ SETTINGS ------

Minimum Voltage (mv) = 1
Minimum V/I (ohm) = 0.0005
Minimum apparent resistivity (ohm-m) = 1
Maximum apparent resistivity (ohm-m) = 100000
Maximum repeat error (%) = 7
Maximum reciprocal error (%) = 10
Remove negative apparent resistivity in ERT data: Yes
Keep All Data (no data removal): No
Inversion Method: Smooth model inversion
Vertical axis: Positive Upward
Y Coordinate = Depth
Min electrode spacing X (m) = 0.003
Min electrode spacing Z (m) = 0.003
Forward Modeling Method: Finite element method
Forward system solver: Cholesky decomposition method

Boundary condition type: Dirichlet
Number cells or elements betwenn two electrodes = 2
Lower-layer-thickness / Upper-layer-thickness = 1.1
Depth of Inverted Model / Depth of Pseudosection = 1.1
Max number of iteration of nonlinear inversion = 15
Stop RMS error = 5%
Mininum error reduction between two iterations = 3%
Stop at Max number of iterations: No
Stop when RMS is small enough: No
Stop when RMS can not be reduced: Yes
Res Data reweighting: No
Use Reciprocal Error: No
Stop when L2 norm is small enough: No
Initial smoothness factor = 100
Roughness conditioner = 0.1
Starting model: Avg AppRes.
Start halfspace resistivity = 8.06 ohm-m
Minimum resistivity = 1.0 ohm-m
Maximum resistivity = 100000.0 ohm-m
Number of elements combined horizontally = 1
Number of elements combined verically = 1
Vertical / Horizontal roughness ratio = 0.2
Estimated noise of resistivity data = 5%
Initial damping factor of resistivity = 100
Starting iteration of quasi Newton method = 20
IP inversion method: No IP Inversion
Terrain mesh transform method: Damped transform.

;------ ELECTRODE LOCATIONS ------

Electrode	X	Y	Terrain_X	Terrain_Y
0,	0.000,	0.000,	0.000,	0.000
1,	4.000,	0.000,	4.000,	-0.029
2,	8.000,	0.000,	8.000,	-0.058
3,	12.000,	0.000,	12.000,	-0.087
4,	16.000,	0.000,	16.000,	-0.122
5,	20.000,	0.000,	20.000,	-0.188
6,	24.000,	0.000,	24.000,	-0.262
7,	28.000,	0.000,	28.000,	-0.341
8,	32.000,	0.000,	32.000,	-0.420
9,	36.000,	0.000,	36.000,	-0.499
10,	40.000,	0.000,	40.000,	-0.581
11,	44.000,	0.000,	44.000,	-0.692
12,	48.000,	0.000,	48.000,	-0.845
13,	52.000,	0.000,	52.000,	-1.023
14,	56.000,	0.000,	56.000,	-1.096

15,	60.000,	0.000,	60.000,	-1.157
16,	64.000,	0.000,	64.000,	-1.210
17,	68.000,	0.000,	68.000,	-1.262
18,	72.000,	0.000,	72.000,	-1.315
19,	76.000,	0.000,	76.000,	-1.367
20,	80.000,	0.000,	80.000,	-1.413
21,	84.000,	0.000,	84.000,	-1.457
22,	88.000,	0.000,	88.000,	-1.502
23,	92.000,	0.000,	92.000,	-1.454
24,	96.000,	0.000,	96.000,	-1.393
25,	100.000,	0.000,	100.000,	-1.347
26,	104.000,	0.000,	104.000,	-1.394
27,	108.000,	0.000,	108.000,	-1.440

May 22, 2013 Survey Parameters

Advanced Geosciences Inc. (AGI) Sting/SuperSting measured data (*.stg) Type: XYZ
A trimmed data set by AGI EarthImager 2D. Version: 2.4.0 (Build 617). Records: 284
Raw data file: C:\Documents and Settings\jpeurifoy\Desktop\Thesis Information\Research Data\Resistivity\5.22.13\4m MRT 5.22.13\BRAD4M_Reversed_Scaled\trial6\BRAD4M_Reversed_Scaled_trial6.stg
Terrain file: C:\Documents and Settings\jpeurifoy\Desktop\Thesis Information\Research Data\Resistivity\5.22.13\4m MRT 5.22.13\TranD12.trn

Number of Data = 284
Number of Electrodes = 28
Number of Surface Electrodes = 28
Number of IP Data = 0

Processing starts at 2013-09-23 09:38:33

;------ SETTINGS ------

Minimum Voltage (mv) = 1
Minimum V/I (ohm) = 0.0005
Minimum apparent resistivity (ohm-m) = 0.1
Maximum apparent resistivity (ohm-m) = 10000
Maximum repeat error (%) = 7
Maximum reciprocal error (%) = 10
Remove negative apparent resistivity in ERT data: Yes
Keep All Data (no data removal): No
Inversion Method: Smooth model inversion
Vertical axis: Positive Upward
Y Coordinate = Depth
Min electrode spacing X (m) = 0.003

Min electrode spacing Z (m) = 0.003
Forward Modeling Method: Finite element method
Forward system solver: Cholesky decomposition method
Boundary condition type: Dirichlet
Number cells or elements betwenn two electrodes = 2
Lower-layer-thickness / Upper-layer-thickness = 1.1
Depth of Inverted Model / Depth of Pseudosection = 1.1
Max number of iteration of nonlinear inversion = 15
Stop RMS error = 5%
Mininum error reduction between two iterations = 3%
Stop at Max number of iterations: No
Stop when RMS is small enough: No
Stop when RMS can not be reduced: No
Res Data reweighting: Yes
Use Reciprocal Error: No
Stop when L2 norm is small enough: Yes
Initial smoothness factor = 100
Roughness conditioner = 0.1
Starting model: Avg AppRes.
Start halfspace resistivity = 8.26 ohm-m
Minimum resistivity = 1.0 ohm-m
Maximum resistivity = 100000.0 ohm-m
Number of elements combined horizontally = 1
Number of elements combined verically = 1
Vertical / Horizontal roughness ratio = 0.2
Estimated noise of resistivity data = 5%
Initial damping factor of resistivity = 100
Starting iteration of quasi Newton method = 20
IP inversion method: No IP Inversion
Terrain mesh transform method: Damped transform.

;------ ELECTRODE LOCATIONS ------

Electrode	X	Y	Terrain_X	Terrain_Y
0,	0.000,	0.000,	0.000,	0.000
1,	4.000,	0.000,	4.000,	-0.029
2,	8.000,	0.000,	8.000,	-0.058
3,	12.000,	0.000,	12.000,	-0.087
4,	16.000,	0.000,	16.000,	-0.122
5,	20.000,	0.000,	20.000,	-0.188
6,	24.000,	0.000,	24.000,	-0.262
7,	28.000,	0.000,	28.000,	-0.341
8,	32.000,	0.000,	32.000,	-0.420
9,	36.000,	0.000,	36.000,	-0.499
10,	40.000,	0.000,	40.000,	-0.581
11,	44.000,	0.000,	44.000,	-0.692

12,	48.000,	0.000,	48.000,	-0.845
13,	52.000,	0.000,	52.000,	-1.023
14,	56.000,	0.000,	56.000,	-1.096
15,	60.000,	0.000,	60.000,	-1.157
16,	64.000,	0.000,	64.000,	-1.210
17,	68.000,	0.000,	68.000,	-1.262
18,	72.000,	0.000,	72.000,	-1.315
19,	76.000,	0.000,	76.000,	-1.367
20,	80.000,	0.000,	80.000,	-1.413
21,	84.000,	0.000,	84.000,	-1.457
22,	88.000,	0.000,	88.000,	-1.502
23,	92.000,	0.000,	92.000,	-1.454
24,	96.000,	0.000,	96.000,	-1.393
25,	100.000,	0.000,	100.000,	-1.347
26,	104.000,	0.000,	104.000,	-1.394
27,	108.000,	0.000,	108.000,	-1.440

APPENDIX B

DATA MISFIT CROSSPLOTS AND DATA MISFIT PSEUDOSECTIONS

June 30, 2012

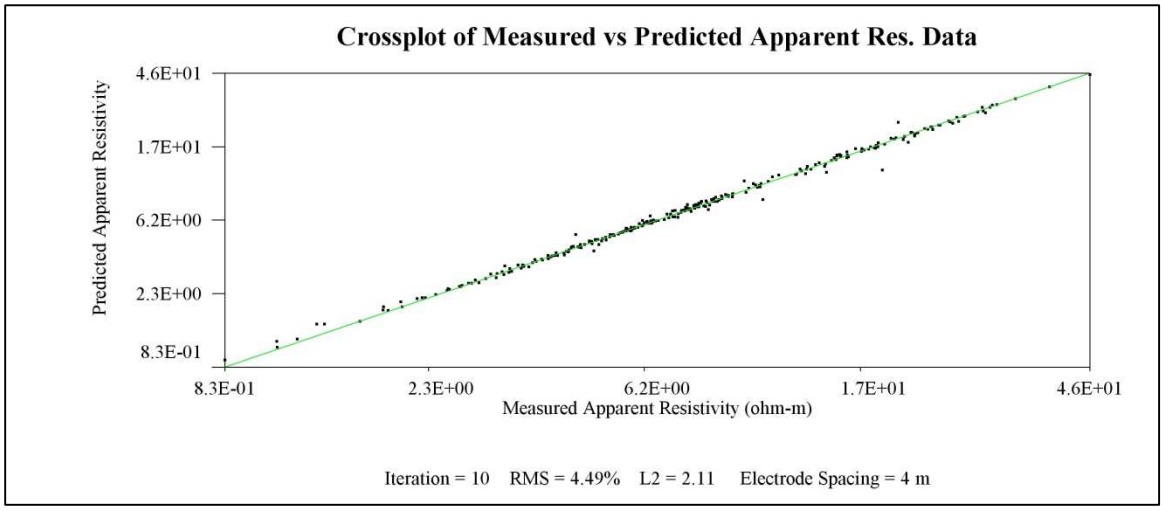

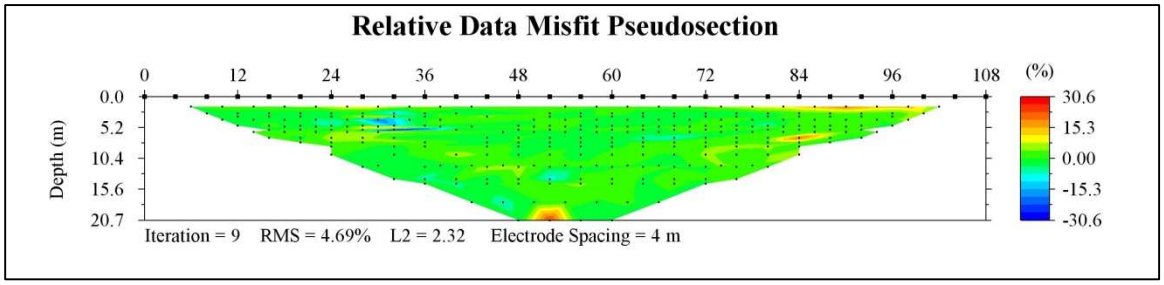

August 1, 2012

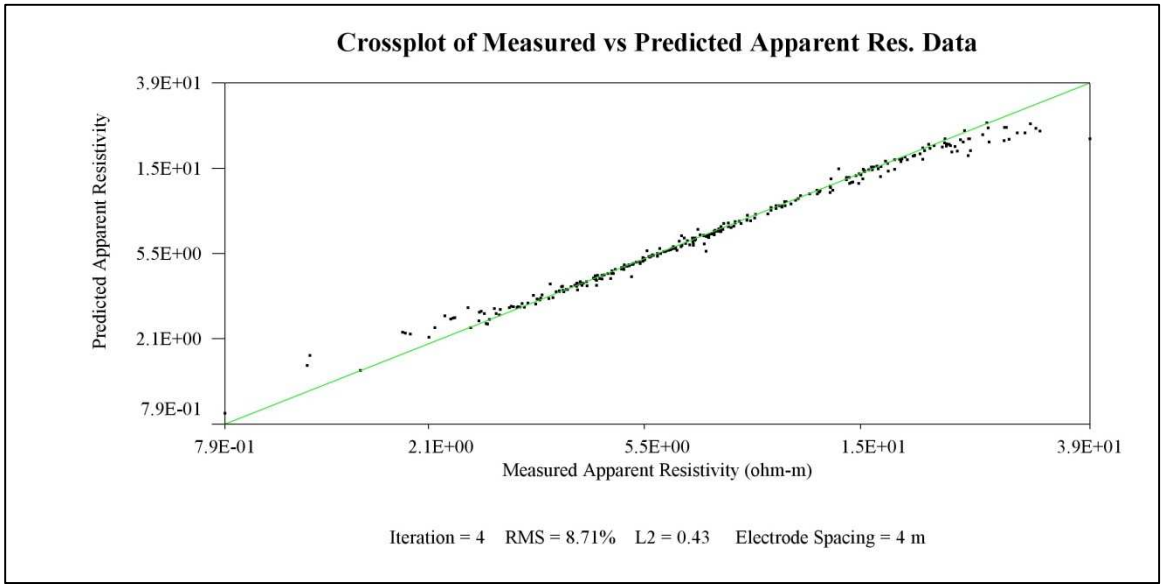

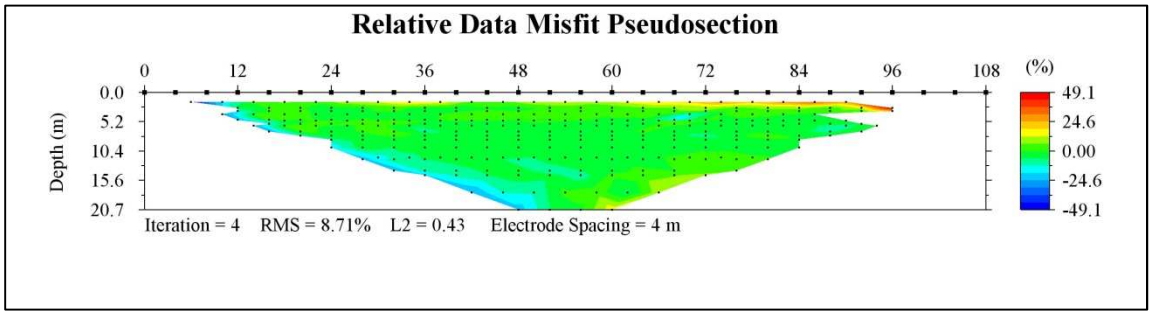

January 11, 2013

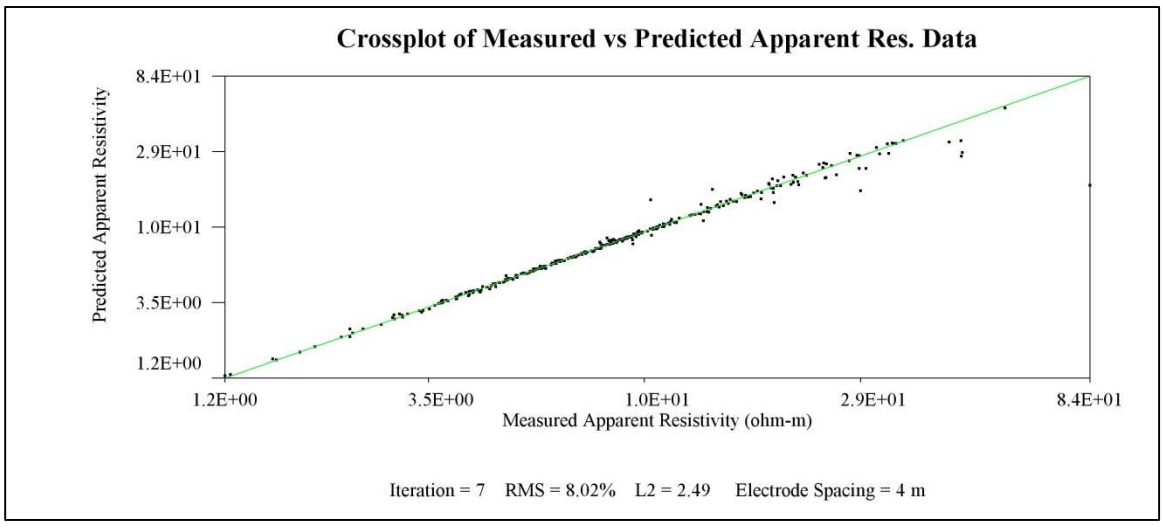

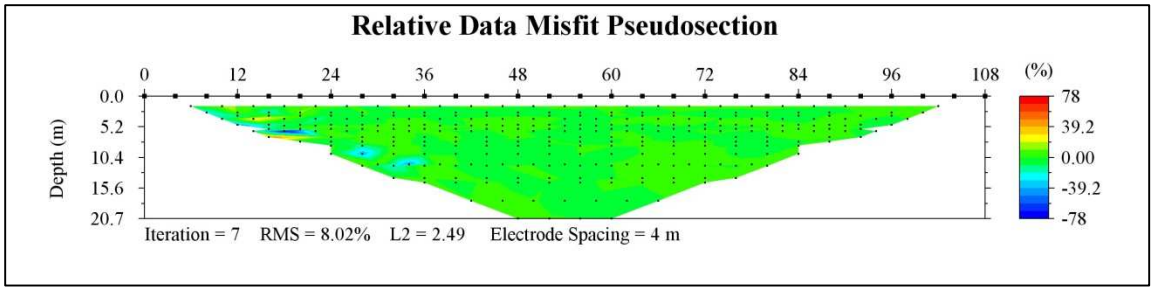
Relative Data Misfit Pseudosection
0
12
24
36
48
60
72
84
96
108
(%)
0.0
5.2
10.4
15.6
20.7
Depth (m)
78
39.2
0.00
-39.2
-78
Iteration = 7 RMS = 8.02% L2 = 2.49 Electrode Spacing = 4 m

May 22, 2013

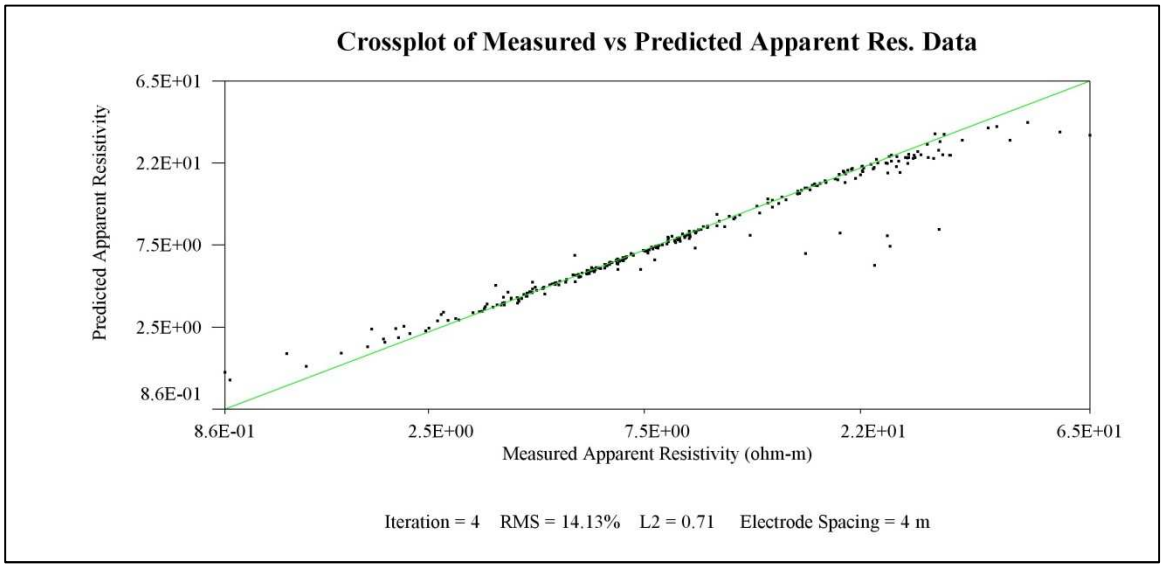
Crossplot of Measured vs Predicted Apparent Res. Data
6.5E+01
2.2E+01
7.5E+00
2.5E+00
8.6E-01
Predicted Apparent Resistivity
8.6E-01
2.5E+00
7.5E+00
2.2E+01
6.5E+01
Measured Apparent Resistivity (ohm-m)
Iteration = 4 RMS = 14.13% L2 = 0.71 Electrode Spacing = 4 m

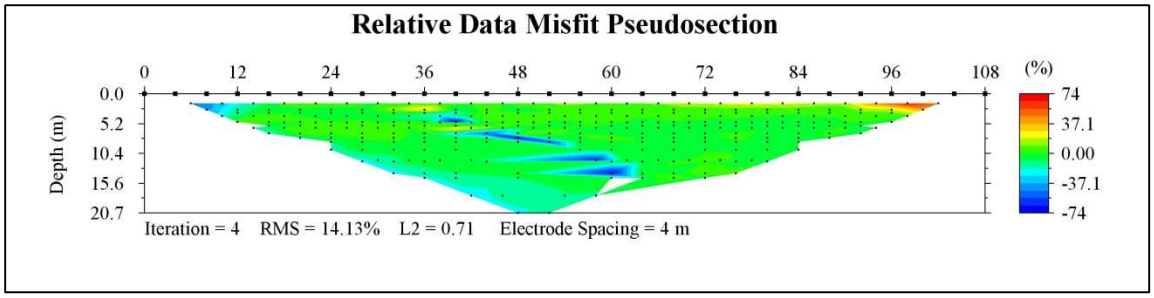
Relative Data Misfit Pseudosection
0
12
24
36
48
60
72
84
96
108
(%)
0.0
5.2
10.4
15.6
20.7
Depth (m)
74
37.1
0.00
-37.1
-74
Iteration = 4 RMS = 14.13% L2 = 0.71 Electrode Spacing = 4 m